



ISEC

*Instituto Superior de Engenharia de Coimbra
Electrical Engineering*

**Development of a Motor Controller for
Electric Bicycles**

*SERHAT KARNAP
21270767*

Project Advisor

*Professor Paulo PEREIRINHA
Eng. Marco SILVA*

Portugal-2018

ABSTRACT

This project aims to develop a BLDC motor controller and assemble it by using friction drive technique to the bicycle. One focus of this objective was designing a motor controller and traction system easy to apply on bicycles. A number of commercial motor control techniques have been investigated for feasibility along with the relevant theory behind controlling BLDC motors. The scope of this project covers power systems, feedback control of brushless DC (BLDC) motors, and input signal conditioning. Another focus of this objective was designing a traction system, which can be made by printing the mechanical part with a 3D printer. This process makes it easy and flexible to assemble the system on different bicycles. Overall, this project provides the core tractive system while providing a solid basis for future projects.

RESUMO

Este projeto visa desenvolver um controlador de motor BLDC e a sua montagem usando a técnica de acionamento por fricção para todas as bicicletas. Um dos focos deste objetivo foi projetar o controlador do motor e a forma de aplicar o sistema de tração de forma simples em bicicletas. Várias técnicas comerciais de controlo de motores foram investigadas para verificar a viabilidade do sistema de acordo com a teoria relevante por detrás do controlo de motores BLDC. O âmbito deste projeto abrange sistemas de energia, controle de realimentação de motores DC sem escovas (BLDC) e condicionamento de sinal de entrada. Outro foco deste objetivo foi projetar o sistema de tração, que pode ser impresso com uma impressora 3D, tornando mais fácil e flexível a montagem em bicicletas diferentes. No geral, este projeto oferece um sistema de tração central, e uma base de estudo sólida para futuros projetos.

Acknowledgments

First and foremost, I wish to thank my supervisors, Prof. Paulo Pereirinha and Eng. Marco Silva for their much appreciated help, as well as Mr. Francisco Dias and Eng. João Queiró for their help with PCB manufacturing. Prof. Paulo Pereirinha and Eng. Marco Silva have been supportive since the days I began working on this project. Ever since, supported me not only by providing a research assistantship, but also academically and emotionally. Through the rough road to finish this project during the most difficult times when writing this thesis, they gave me the moral support and the freedom I needed to move on. Their words could always inspire me and keep me motivated. Without their kind and patient instruction, it would be impossible for me to finish this project. Thank you!

CONTENTS

ABSTRACT	2
RESUMO	2
Acknowledgments.....	3
List of Figures.....	6
List of Tables.....	8
LIST OF ACRONYMS	9
CHAPTER 1.....	10
INTRODUCTION	10
Project Objectives	11
Historical overview of the electric bicycle	11
Related standards and regulations about electric bicycle	15
CHAPTER 2.....	19
Electric bicycle model and simulation.....	19
Electric bicycle simulation	20
Choosing the motor type and power	24
CHAPTER 3.....	25
Brushless Electric Motors (BLDC)	25
Permanent magnet BLDC motors.....	25
Types of brushless motors	25
In-Runner motors	26
Out-Runner motors	26
CHAPTER 4.....	28
Brushless DC (BLDC) motors and sensorless drives	28
Open loop control	30
Closed loop control	31
Sensorless BLDC motor driving systems.....	32
Types of back EMF detection schemes	32
Direct Back EMF Detection using an ADC input	34
PM-BLDC motor position detection sensored or sensorless	36
Detecting motor angular position with Hall Effect sensors	36
Detecting the back EMF strategies to improve back EMF Detection	37
PWM technique.....	38

Chopping current control	38
Conventional 120° PWM	40
Technique of virtual neutral point	41
Other sensorless techniques estimation and Model-Based methods.....	41
CHAPTER 5.....	43
Electric Bicycle Project Implementation	43
Purposed traction drive of this report	43
Designing the main schematic	44
BLDC motor driver board (Version 1.0).....	45
Voltage regulator.....	45
High and low side drivers	45
First test and controlling	47
Version (1.0) driver board conclusions	48
BLDC motor driver board (Version 2.0).....	49
Version (2.0) driver board conclusions	51
BLDC motor driver board (Version 3.0).....	52
DC-DC Isolator	55
The BLDC back EMF detection software	57
Conclusion of back EMF BLDC sensorless motor drive	59
CHAPTER 6.....	60
Development of a Sensored BLDC motor drive	60
Version 1.0 BLDC sensored motor driver	62
Version (2.0) BLDC sensored motor driver.....	64
The main contactor circuit	65
Final test and assembly	66
CHAPTER 7.....	68
Conclusions and Future Work	68
REFERENCES	69
APPENDIX	73
Software for sensored BLDC motor	73

List of Figures

Figure-1 Sales evolution of the electric bicycles [3]	10
Figure-2 Historical Overview of bicycle [8]	12
Figure-3 Hub motor patents [8]	13
Figure-4 Steffens electric bicycles [9].....	13
Figure-5 Schnepf electric bicycles friction drive [9]	14
Figure-6 Dubé's electric bicycles [10].....	14
Figure-7 Power profiling of cycling	17
Figure-8 The forces acting on the electric bicycle on an sloped road [15]	19
Figure-9 Simulation results [16]	21
Figure-10 Simulation parameters of drivetrain [16]	21
Figure-12 Demagnetization curves of various permanent magnet materials [19]......	23
Figure-13 In runner and out runner types [17]	26
Figure-14 BLDC Motor driving sequence [22]	29
Figure-15 Open loop control block diagram [30]	30
Figure-16 Closed loop control block diagram [30]	31
Figure-17 PI controller block diagram [30]	31
Figure-18 The phase current is in phase with the back EMF in BLDC motor [32]	32
Figure-19 (A) Back EMF zero crossing detection scheme with the motor neutral point (B) back EMF zero crossing detection scheme with the virtual neutral point.	33
Figure-20 Circuit model of BLDC motor	34
Figure-21 Hall Effect sensors in hub motor [35]	37
Figure-22 PWM Algorithm [38]	38
Figure-23 Current chopping technique [40].....	39
Figure-24 Three Phase Brushless motor control sequence with current chopping [41]	40
Figure-25 PWM Conventional 120° PWM [38]	40
Figure-26 Back EMF detection with neutral point and LPF [42]	41
Figure-27 Example of advance techniques of ANN [53]	42
Figure-28 Purposed traction system for BLDC electric bicycles.....	43
Figure-30 The complete schematic of the motor controller.....	45
Figure-31 MOSFET schematic explanation (V_{th} = Threshold).....	46
Figure-32 MOSFET driver representation	46

Figure-33 3D model of motor controller	47
Figrue-34 First test setup	47
Figure-35 Adding resistors to each phase	48
Figure-36 Version 2.0 controller board	49
Figure-37 New current limiting resistor configuration	50
Figure-38 PWM scope outputs of 2 phases 100% throttle	50
Figure-39 Current measuring from main DC-Bus.....	51
Figure-40 Version (3.0) controller board	52
Figure-41 Opto-coupler schematic.....	53
Figure-42 First test of the Optic Isolators	53
Figure-43 Opto-coupler frequency testing.....	54
Figure-44 Max Opto-coupler frequency before get in the saturation	54
Figure-45 3D schematic BLDC driver board V3.0	55
Figure-46 Version (3.0) BLDC motor controller.....	56
Figure-47 Test setup of Version (3.0).....	56
Figure-48 Zero crossing point calculations.....	57
Figure-49 Cases of MOSFETs controlling sequence	57
Figure-50 Comparing the zero crossing	58
Figure-51 The reading the potentiometer value.....	58
Figure-52 Commercial ESC phase scope output 50% throttle	59
Figure-53 Sensor replacement to the motor stator.....	60
Figure-54 Hall sensors replacement from motor stator	60
Figure-55 Commutation sequence according to the Hall sensors outputs [55]	61
Figure-56 Sensored BLDC motor driver schematic version (1.0)	62
Figure-57 3D View of Version (1.0)	63
Figure-58 First setup for Version (1.0)	63
Figure-60 Schematic of BLDC sensored motor driver version (2.0).....	64
Figure-61 Due to time limitations this new version was made on a prototyping board.....	64
Figure-62 First test setup of sensored motor driver V2.0.....	65
Figure-63 The main contactor circuit.....	65
Figure-64 The final design	66
Figure-65 The final system of sensored motor	67

List of Tables

Table-1 Legitimate electric bicycle limits set in various countries [11] 15

LIST OF ACRONYMS

- ADC - Analogue to Digital Converter
- Ain - Analogue Input
- ASDs - Adjustable Speed Drivers
- BLDC - Brushless DC Motor
- BEV - Battery Electric Vehicles
- CAN - Controller Area Network
- Din - Digital Input
- DTC - Direct Torque Control
- EKF - Extended Kalman Filter
- EMDs - Electronic Motor Drivers
- EMF - Electromagnetic Force
- ECU - Electronic Control Unit
- FPGA- Field Programmable Gate Array
- IM - Induction Motor
- MOSFET – Metal Oxide Surface Field Effect Transistors
- HVAC – Heating, Ventilation, and Air Conditioning
- HEV - Hybrid Electric Vehicles
- Hin - High Input
- Lin - Low Input
- MP - Microprocessors
- rpm - Rotation Per Minute
- PWM - Pulse Width Modulation
- PMSM - Permanent Magnet Synchronous Motor
- PAEB - Pedal Assisted Electric Bicycles

CHAPTER 1

INTRODUCTION

Bicycles are cheap, clean, quiet and can reduce traffic problems making them a promising option for urban transportation. A person can ride a bicycle 2 or 3 times faster using the same energy that would consume while walking. This feature makes the bicycle the most efficient vehicle [1].

Riding a bicycle has important benefits of the human health. According to the WHO study, cycling 30min every day has increases the human life by eight years [2].

However, cycling is not as comfortable as driving a car or riding a scooter making cycling less popular. Electric powered bicycles can help with an electric motor allowing the cyclist to travel longer distances and allow to easily climbing road slopes. Today's number of electric powered bicycles has been increasing rapidly. According to Electric Bike World Report 2012 in Figure-1, by 2018, it was expected that annual electric bicycle sales worldwide will reach 48,000,000.

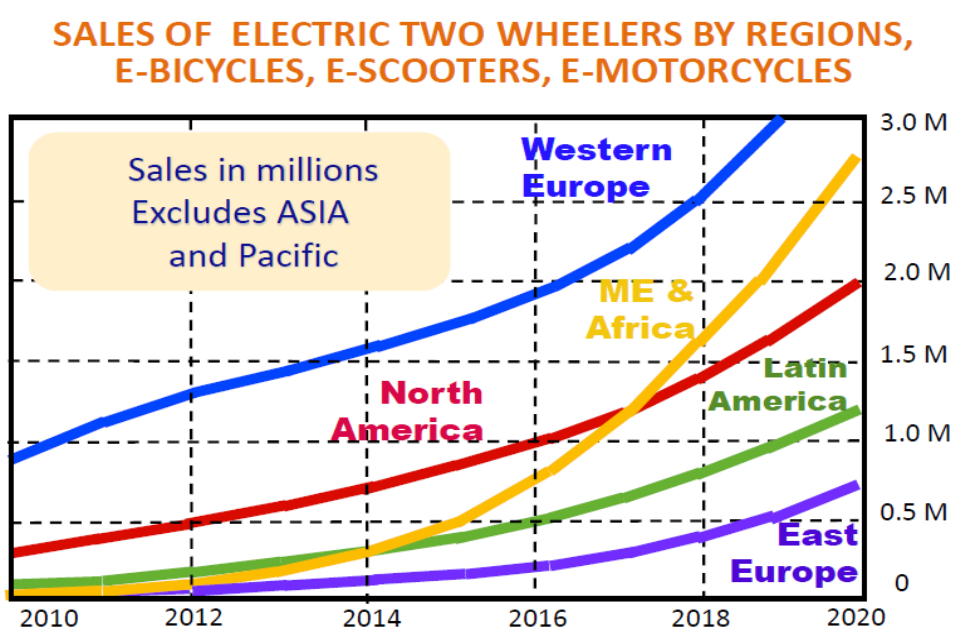


Figure-1 Sales evolution of the electric bicycles [3]

Pedal Assisted Electric Bicycles (PAEB) are hybrid vehicles. PAEB combines human power and electric power. This feature of electric bicycles reduces human dependence. In hilly areas where cycling is difficult, electric power support makes riding easy, using much less energy and cycling at the same speed. This feature allows enjoyable cycling. With electric power assist regardless of age or condition, a lot of more people can benefit from riding bicycles. This way, cycling can be considered not only for sports or fun, but also as a means of transportation.

Electric bicycles uses electric motor, its driver and battery systems. Three different types of electric motor assembly are widely used in bicycles: in the front-wheel, rear-wheel or pedal-mounted. Usually to balance the center of mass, the motor installation on electric bicycles, for hub-motorized systems the front or rear wheel mount are preferred. Front drive systems have a poor downhill performance and dangerous situations can happen while breaking. Rear drive systems have better performance for hill and are more suitable for light vehicles [4].

Hub motor drive systems have many advantages as well as ease of manufacture and space saving on the bicycle but assembly part still requires professional help.

The purposed traction system is suitable for low-speed and high-torque operation. This system aims to eliminate the mechanical transmission losses because it does not require a gear or mechanical converter. This system, which allows same feature as e-bikes on the market regenerative braking in the case of downhill braking increases the driving range. Another important feature of direct driving is the ability to balance the vehicle center of mass, and its light traction system features lower the power consumption.

For this project, it will be used a commercial out-runner BLDC motor. This out-runner BLDC motor usually is used on the UAV (Unmanned Aerial Vehicle) systems. Out-runner BLDC motors due to their high efficiency, high power/mass rate and basic designs makes them suitable for electric powered applications. It will be used 3D CAD/CAM simulations for mechanical design which can apply to different bicycle brand on the market.

Project Objectives

An electric bicycle can be defined as a system consisting essentially of an electric motor, a motor drive and a battery. Although, there are a wide variety of designs, patents and commercially available products for electric bicycles that can be find on the internet. The electric motor, converts the electric energy to mechanical energy, and is the component that most influences the performance and efficiency of the system. For this reason, it is very important to choose the appropriate driving system for the design of electric bicycle systems.

In this study, it was aimed to design a motor controller for BLDC motors and select the lightest BLDC motor on market for electric bicycles, to convert battery energy to wheel motion in an efficient and easy way. In this direction, the requirements of the electric bicycle system are analyzed, and the design of the motor driver it will be studied.

Using computer-aided simulations, an appropriate BLDC motor on the market, considering tractive power, will be chosen, and the motor installation performance evaluated from the obtained results.

Historical overview of the electric bicycle

It is thought that the first bicycle, in its primitive meaning, appeared in China in the 12th century [5]. The first reliable known source in the history of bicycles is from 1817. A two wheeled wooden vehicle invented by the German Baron Karl von Drais de Sauerbrun, provided motion support, and he was considered a bicyclist. Drais received a patent in 1818 for the invention of the name "laufmaschine" which means "jogging machine" in German. This vehicle, which became known as "velespit" in Western Europe and America in a short time, is known as "hobby horse" or "snobber" among the public. Although it was an alternative to horse-drawn carriage and could not reach high speeds, it was banned in 1821 due to the increase of accidents. Since the countries where velesipit existed developed in this period were under the effect of rail transportation, no significant progress has been made in cycling until the 1860s [6].

In 1866, the French Pierre Michaux and Pierre Lallement laid the foundations for a modern bicycle with front wheel pedal design, as shown in Figure-2. Over time, bicycle designs have

been created with various wheel sizes and different forms. The high front wheel model, which was developed in 1870, is one of the outstanding designs of bicycle history.

In 1885, with John Dunlop's chain drive system and pneumatic tires, the bike became a reliable and comfortable means of transportation. Many technologies, such as ball bearings, pneumatic tires, chain stretching gear, developed for bicycles, have played a major role in the development of both motorcycles and automobiles. In this regard, cycling can be seen as the starting point of individual transportation technologies [7] [8].

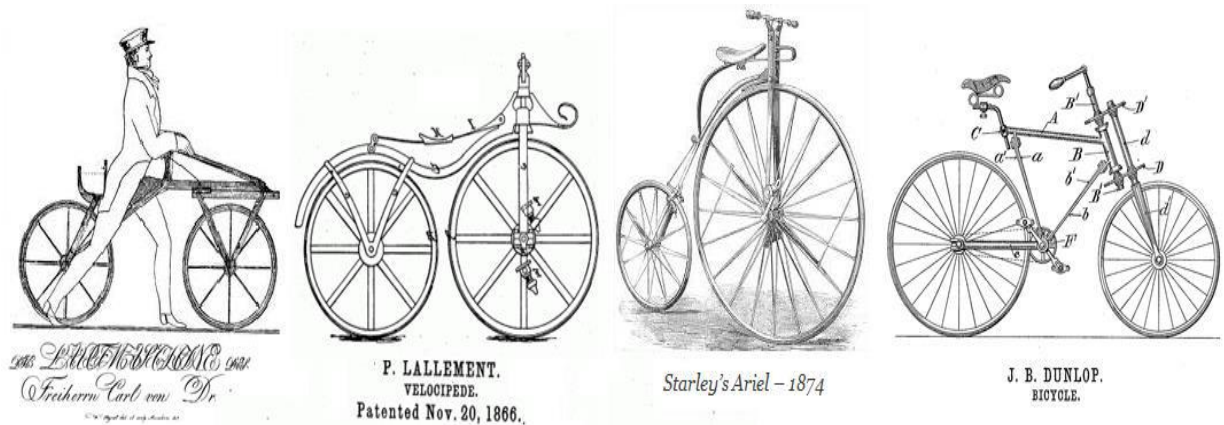


Figure-2 Historical Overview of bicycle [8]

Until the end of the 19th century, there was a great deal of interest in cycling, especially in Western European countries. The reason for the higher interest rate compared to America is that the distance between settlements is shorter in Europe. With the increase of factories and the positive effect of mass production on the costs, the number of bicycles has reached to massive amounts.

By the end of the nineteenth century, in Europe it had become a vehicle used for bicycle sports and weekend excursions. Although the bikes had taken their place in the streets again due to the lack of oil during World War II, the tendency to cycling has diminished once again. On the other hand, in underdeveloped countries, bicycle is seen as a means of transportation and necessity [7].

Wellington Adams, Albert Parcell and Edward Parkhurst are the foundations of two-wheel electric vehicle technology. Wellington Adams create the first in wheel motor (hub) in 1884 as illustrated in Figure-3. Adams designed a motor that is connected to the wheel via a complex gear system [8]. Albert Parcell's patented design in 1890 is the first hub to be applied on a car. Edward Parkhurst has also patented the first low-speed high-torque electric hub engine.

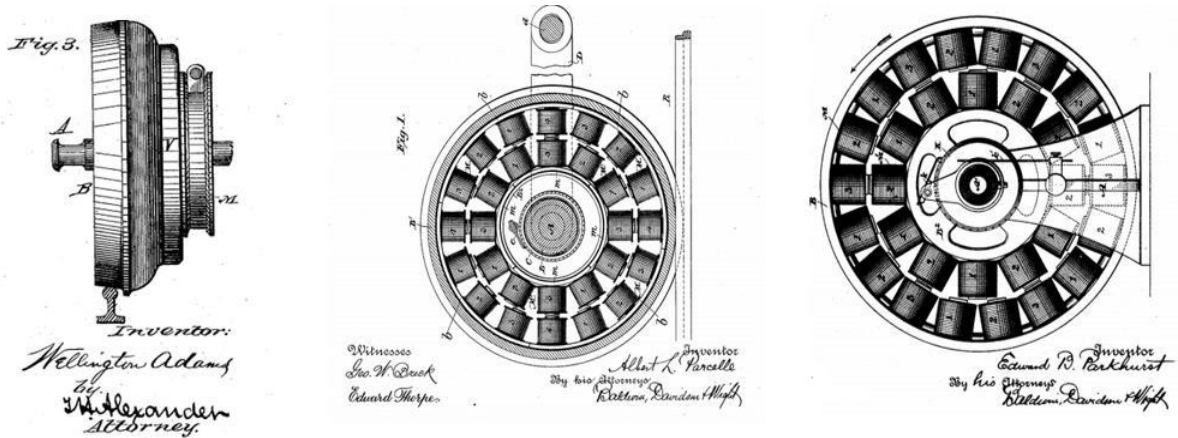


Figure-3 Hub motor patents [8]

The patent, taken by Ogden Bolton in 1895, is the first patent for electric bicycle. Bolton has a patented permanent magnet motor with a 6-pole permanent magnet, powered by a 100 V-10A battery. The brush direct current motor was placed in the rear wheel. There is no gear system or mechanical converter in the motor. Despite being the first known patent, Bolton's carries traces similar to today's electric bicycles. Mathew J. Steffens, in his patent in 1898, describes a system that provides driving with an electric motor connected via a rear wheel strap. The motor was placed in the saddle boring. The mechanical energy is transmitted via a chain to the rear wheel so that the rear wheel was supported by the motor support thanks to the belt pulley system. Steffens stated that this system could also be used on tricycles and similar vehicles as seen in Figure-4 right [9].

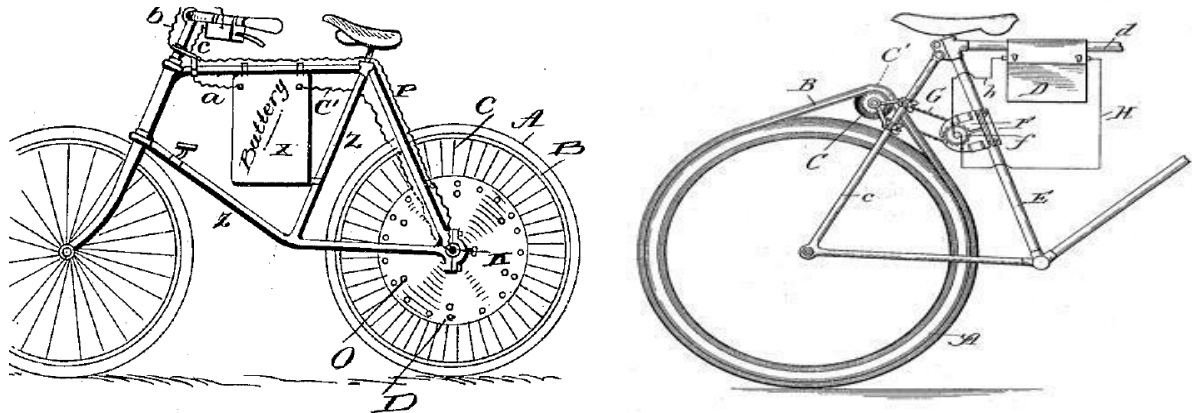


Figure-4 Steffens electric bicycles [9]

John Schnepf's electric bicycle design in 1899 was based on the principle that the electric motor mounted on the rear of the rear wheels touches the wheel and makes the bicycle move with the effect of friction (see in Figure-5). Schnepf noted that in the event of a downhill, the engine would charge the battery by acting as a dynamo, but the battery still needs to charge under normal charging conditions. However, this system was ineffective on rainy days. Due to water, friction between belt and motor is reduced causing traction losses.

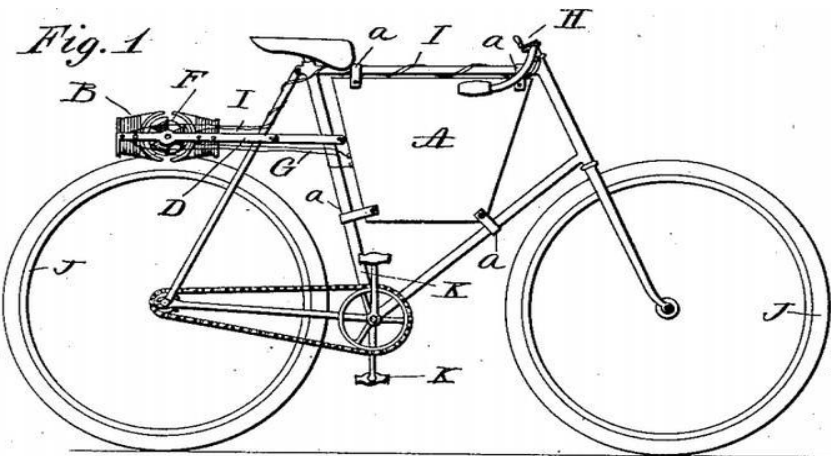


Figure-5 Schnepf electric bicycles friction drive [9]

The patents on the use of torque sensor and motor control have emerged at the end of 1990's.

In a 2005 patent from Jean-Yves Dubé, a useful solution for torque sensing using a strain gauge sensor to engage engine support as described in Figure-6 is exhibited. The sensor, positioned vertically on the shaft of the motor in the rear wheel hub, generates a signal by measuring the torsion of the mover by the driver pedaling. The motor enters the traction mode with the strain information sent by the processor in real time via the filter, amplifier and analog-to-digital converter, and motor support provided as the pedal pressure ratio of the driver [10].

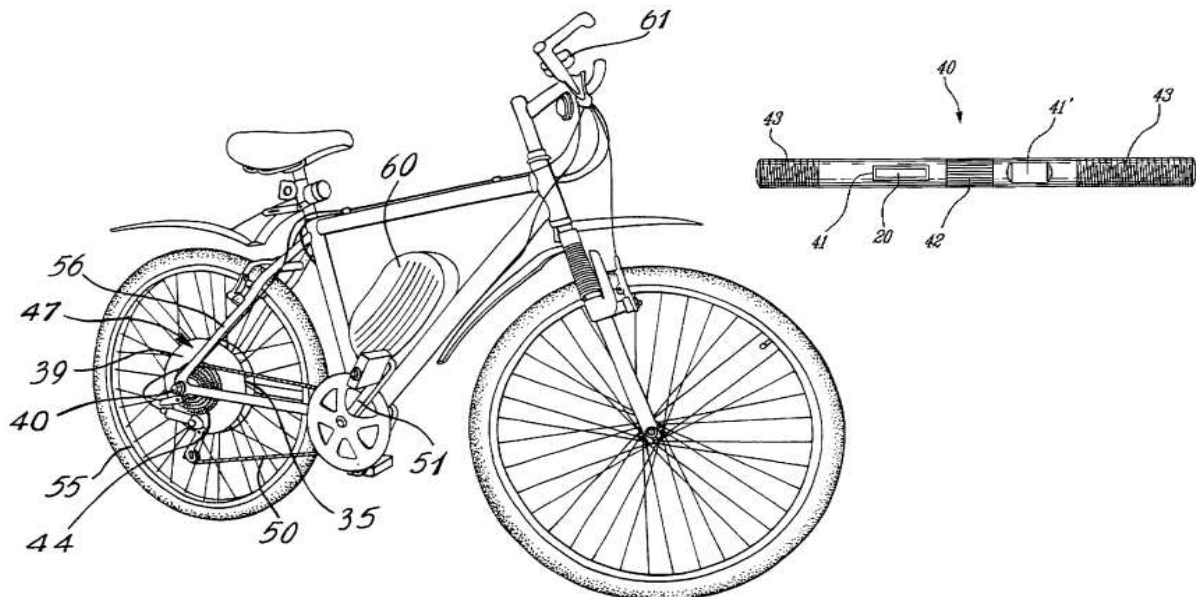


Figure-6 Dubé's electric bicycles [10]

Today, electric bicycles are sold as a commercial product. In the fast growing electric bicycle market, there are products of various price ranges and technology levels. Electric bicycles mainly consisting of electric motor, driver circuit and battery also have various sensors and dashboard displays depending on their development.

These components are sold in assembled bicycles, as well as in kits that can be sold separately to enable the user to convert the existing bicycle into an electric bicycle. Electric bicycle conversion kits are mostly composed of a jumper motor, battery, control circuit and connection elements.

Related standards and regulations about electric bicycle

Along with the increasing popularity of electric bikes, many countries have set legal limits on how motor power, speed, weight and engine support will be activated. The standards that countries have established depend on performance and security approaches. The legal electric bicycle limits for electric bicycles in various countries are summarized in Table-1. Standards and regulations are the most important factors in determining the basic design parameters of the system.

Country/Region	Motor Power Limit [W]	Speed Limit [km/h]	Weight Limit [kg]	Others Limitation
<i>European Union</i>	250	25	No Limitation	Pedal Assisted
<i>Britain</i>	200	25	40	Pedal and on / off switch
<i>Canada</i>	500	32	No Limitation	Pedal, on / off button and maintain less than 4 wheels
<i>Taiwan</i>	No Limitation	30	40	No Limitation
<i>Japan</i>	No Limitation	24	No Limitation	No Limitation
<i>China</i>	240	20	No Limitation	No Limitation
<i>America</i>	750	32.2	No Limitation	Pedal, on / off button and maintain less than 4 wheels

Table-1 Legitimate electric bicycle limits set in various countries [11]

Electric bikes are divided into two types according to the input types of the power supply support: 1) Electric bicycles with only supply power to the motor to pedal assist, this system work as a support (PAEB). 2) Electric bicycles with only the motor is powered and no pedal assisting.

PAEB are hybrid vehicles that combine human and motor power. For these types of electric bicycles, a torque sensor or hall sensors must be added to the system that detects when the driver is pedaling. Motor support must only be engaged when the driver is pedaling and must be interrupted when the pedaling is stopped. As an example it can be given the mid drive. The EN15194 is the standard Specification for pedal-assisted electric bicycles in the Europe. According to the standard, the maximum continuous nominal power of the system must be 250 W and the support power must be decreased when the bicycle exceeds the speed of 25 km/h. The, the driver must use his own effort to reach higher speeds.

Support should only be engaged when the driver is pedaling, and the motor must stop providing assistance when the driver releases the pedal. The system voltage is limited to 48 V for safety reasons [11].

There are many researches to measure the power of people during bicycle riding. It is possible to determine the work done during the course by establishing a relationship between "breathing rate meter" and "work-oxygen consumption". In addition to this, there is many data obtained from experiments made in laboratory conditions with a measuring instrument called an ergometer.¹

Human bicycle performance researches are usually conducted with different experimental groups. Since each individual's muscle mass, body structure, and conditional state will be different, it is difficult to generalize about the output obtained from these studies, and each individual's power-time curve is unique. The output power of cyclists is shown in Figure-7. ¹

¹ <http://myworldfromabicycle.blogspot.com/2011/09/comparative-measurements-of-maximal.html>

Maximal Output for Cyclists																																	
Men @ 73kg (161lbs)								Women @ 65kg (143lbs)																									
	unassisted max sprint (200m, mph)		5 second max (watts)		1 minute max (watts)		5 minute max (watts)		Lactate threshold (watts)		VO2 Max (ml/kg/min)		predicted 40k tt avg speed (mph)		predicted 40k tt results (minutes)			unassisted max sprint (200m, mph)		5 second max (watts)		1 minute max (watts)		5 minute max (watts)		Lactate threshold (watts)		VO2 Max (ml/kg/min)		predicted 40k tt avg speed (mph)		predicted 40k tt results (minutes)	
	41.66	1754.92	839.5	554.8	467.2	89.08	31.86	46.8	41.34	1715.5	822.71	539.47	454.06	86.812	31.53	47.28	41.17	1695.06	814.68	532.17	447.49	85.732	31.36	47.54	36.78	1220.05	586.3	411.45	353.6	75.364	30.47	48.93	
World class (e.g., international pro)	41.5	1735.21	831.47	547.5	460.63	88	31.7	47.04	40.8	1756.07	764.31	486.91	408.8	79.036	30.38	49.08	40.41	1675.35	805.92	524.87	440.92	84.652	31.21	47.77	36.64	1206.4	580.45	405.6	348.4	74.392	28.7	51.95	
Exceptional (e.g., domestic pro)	40.84	1655.64	797.89	516.84	435.08	83.464	31.05	48.01	39.98	1556.36	755.55	479.61	402.23	77.956	30.19	49.39	39.81	1536.65	747.52	471.58	395.66	76.768	30.01	49.68	35.6	1108.25	538.85	363.35	311.35	67.372	27.55	54.11	
Excellent (e.g., cat. 1)	40.67	1635.93	789.13	509.54	428.51	82.384	30.89	48.27	39.64	1516.94	738.76	464.28	389.09	75.688	29.83	49.98	39.46	1497.23	730.73	456.98	382.52	74.608	29.65	50.28	35.44	1093.95	533	357.5	305.5	66.4	27.36	54.49	
Very good (e.g., cat. 2)	40.5	1616.22	781.1	502.24	421.94	81.304	30.72	48.54	39.27	1476.79	721.97	448.95	375.95	73.42	29.57	50.6	39.09	1457.08	713.94	441.65	370.11	72.34	29.3	50.89	34.97	1052.35	515.45	339.3	289.9	63.376	26.84	55.55	
Good (e.g., cat. 3)	38.91	1437.37	705.18	434.35	363.54	71.26	29.11	51.22	38.73	1417.66	697.15	426.32	356.97	70.072	28.92	51.55	38.54	1397.95	688.39	419.02	350.4	68.992	28.73	51.9	34.48	1010.1	497.9	321.1	273.65	60.352	26.28	56.74	
Moderate (e.g., cat. 4)	38.35	1377.51	680.36	411.72	343.83	67.912	28.53	52.26	37.97	1338.09	663.57	396.39	330.69	65.644	27.92	53.4	37.78	1318.38	654.81	389.09	324.12	64.564	27.92	53.4	33.81	956.8	492.05	315.25	268.45	59.38	26.1	57.13	
Fair (e.g., cat. 5)	38.16	1357.8	671.6	403.69	337.26	66.724	28.33	52.63	37.38	1278.23	638.02	373.76	311.71	62.296	27.53	54.16	37.58	1298.67	646.78	381.06	317.55	63.376	27.71	53.8	33.64	939.9	468.65	291.2	247	55.384	25.31	58.91	
Untrained (e.g., non-racer)	35.93	1139.53	579.62	320.47	265.72	54.412	25.96	57.43	33.78	1238.81	621.23	368.43	298.57	60.028	27.1	55.02	36.57	1199.39	604.44	343.1	285.43	57.76	26.65	55.94	32.76	870.35	438.75	281.3	220.35	50.416	24.26	61.46	

Figure-7 Power profiling of cycling¹

Although very high power levels can be achieved for a short time period during cycling (1500W for a strong man), the driver starts to get tired in a few seconds. Generally a power level of 500W for a few minutes is possible for a powerful driver. For about an hour, the cycling power can be trained at 350 W, while at the 250 W a powerful person can drive all day. When the results of healthy people are evaluated, a 2-12 min. typical power range between 200-400W is measured. The short-term power values are determined by the mass of the bicycle's driver; 2-4 W/kg for non-fit people, 6-10 W/kg for cyclists, and 10 W/kg for champion cyclists [12].

In this case, the bicycle user power consumption in average for Europe with a weight average of 70.8 kg is approximately 212.4 Watt. When studies on human-bicycle performance are examined, it is seen that the maximum rated power of 250 W for pedal-assisted electric bicycles in the European Standard EN 15194 and Highway Traffic Law 2918 is an appropriate level for evaluating these vehicles in the bicycle class.

Electric bicycle related work

In the work entitled "External-Rotor 6-10 Switched Reluctance Motor for an Electric Bicycle" published by Jianing Lin, N. Schofield and A. Emadi published in 2013, it is mentioned that the electric bicycle market is rapidly growing and that the European manufacturers, who have difficulties in competing with China, have a need for a simple, low cost motor type with high power density. It has been noted that electric bicycle systems can be met with common reluctance motors because of the low efficiency of brushless motors and the high magnet costs of brushless motors, which are commonly used with brushless and brushless direct current motors [13].

In the work entitled "Comparison of Permanent Magnet Brushless Motor with Outer and Inner Rotor Used in E-Bike" by Chlebosz, W., Ombach G., and Junak, J. published in 2010, brushless synchronous motors are theoretically and experimentally compared. The rated power output of the electric bike motor analyzed is 250 W, and the rim on which the motor is mounted is 26 inches. The work consisted of 18-slots and 20-pole brushless synchronous motor with permanent magnet outer rotor. The use of an internal rotor permanent magnet brushless synchronous motor for commercial products has been proposed, demonstrating that the inner rotor motor topology allows the use of cheaper flat magnets [14].

EA Lomonova, AJA Vandenput, J. Rubacek, B. d 'Herripon, and G. Roovers, published in 2002 "Development of an Improved Electrically Assisted Bicycle", a comprehensive study of electrical bicycle mechanical, electromechanical, electromagnetic and control systems. The prototype can provide a max power to the motor of 250 W, maximum speed is 25 km / h and maximum torque support is 50%. The battery voltage was selected as 36 V. In this scope, three types of motor topology with radial flow permanent magnet, axial flow permanent magnet and without slots (surface wound) were examined and design and analysis studies were carried out. Because of the evaluation, a radial flow permanent magnet brushless motor driven by square wave current was selected for the electric power assisted bicycle prototype. This motor type is said to be a low-cost and more reliable system compared to others [15].

CHAPTER 2

Electric bicycle model and simulation

The electric bicycle model and simulation are very important for drive system design to determine the performance of various speed, acceleration, load and road conditions. The electric bike model has been set up to determine the electric bike performance and to obtain the torque and speed values that the system will need under different driving conditions. Thus, the motor to be designed has been investigated with the potential to respond to dynamic effects.

The bicycle needs traction force (F_{tr}) to move forward. The traction force must overcome the rolling resistance force (F_r), the air resistance force (F_{ad}), the climbing force (F_h), and allow the bicycle to move and accelerate (F_a). A dynamic model is shown in Figure-8. Dynamic models are developed based on the effects of these fundamental forces on the system [15].

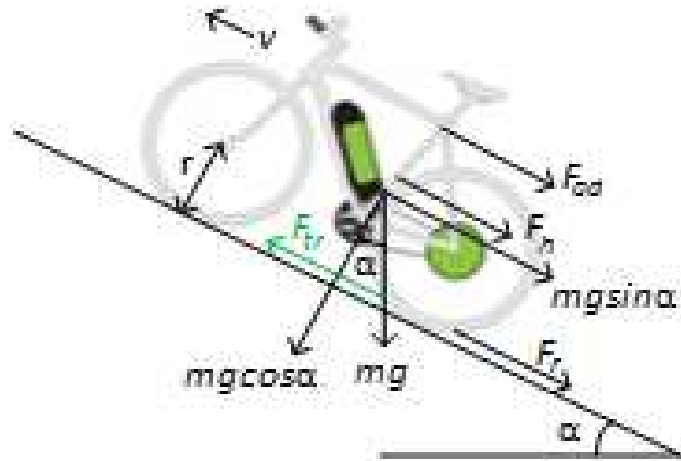


Figure-8 The forces acting on the electric bicycle on an sloped road [15]

As the first step of the bicycle model, the formula of the traction force is defined by the formula in (2.1).

$$F_{tr} = F_r + F_{ad} + F_h + F_a \quad (2.1)$$

Friction resistance is created by bicycle wheel friction. The rolling resistance force is a function of the bicycle weight (m) and the rolling resistance coefficient (F_r), which is dependent on the tire type and the pressure of the tire.

$$F_r = F_r * m * g \quad (2.2)$$

The friction on the bicycle moving thought the air creates the aerodynamic resistance force. This force is proportional to the front surface area (A), the air friction coefficient(C_d), the air density (ρ) and the square of the bicycle speed (V).

$$F_{ad} = \frac{1}{2} * \rho * A * C_d * V^2 \quad (2.3)$$

The hill climbing force equals the component of the bicycle weight in the direction of the slope. This component has a negative value in the case of downhill movement.

$$F_h = m * g * \sin(\alpha) \quad (2.4)$$

In the event of a change in speed, the vehicle needs extra power for acceleration. If the vehicle slows down, this force will be negative.

$$F_a = m * a \quad (2.5)$$

Depending on the parameters given in Formula 2.1, the electric bicycle model is created. In the model, the acceleration of the vehicle is neglected.

Electric bicycle simulation

To run simulations to evaluate the performance of an electric bike the simulator² was used. Moreover, results are shown in Figure-9.

Finding motor brand and specifications in the software options also choosing a proper battery in simulations option and motor driver, simulations parameter's complete for testing.

Choosing the parameters, the simulation will give us a maximum speed, range, power, efficiency and torque requirement.

The simulation it was used for the 250W sensored motor as illustrated at Figure-53.

² <http://www.ebikes.ca/tools/simulator.html>

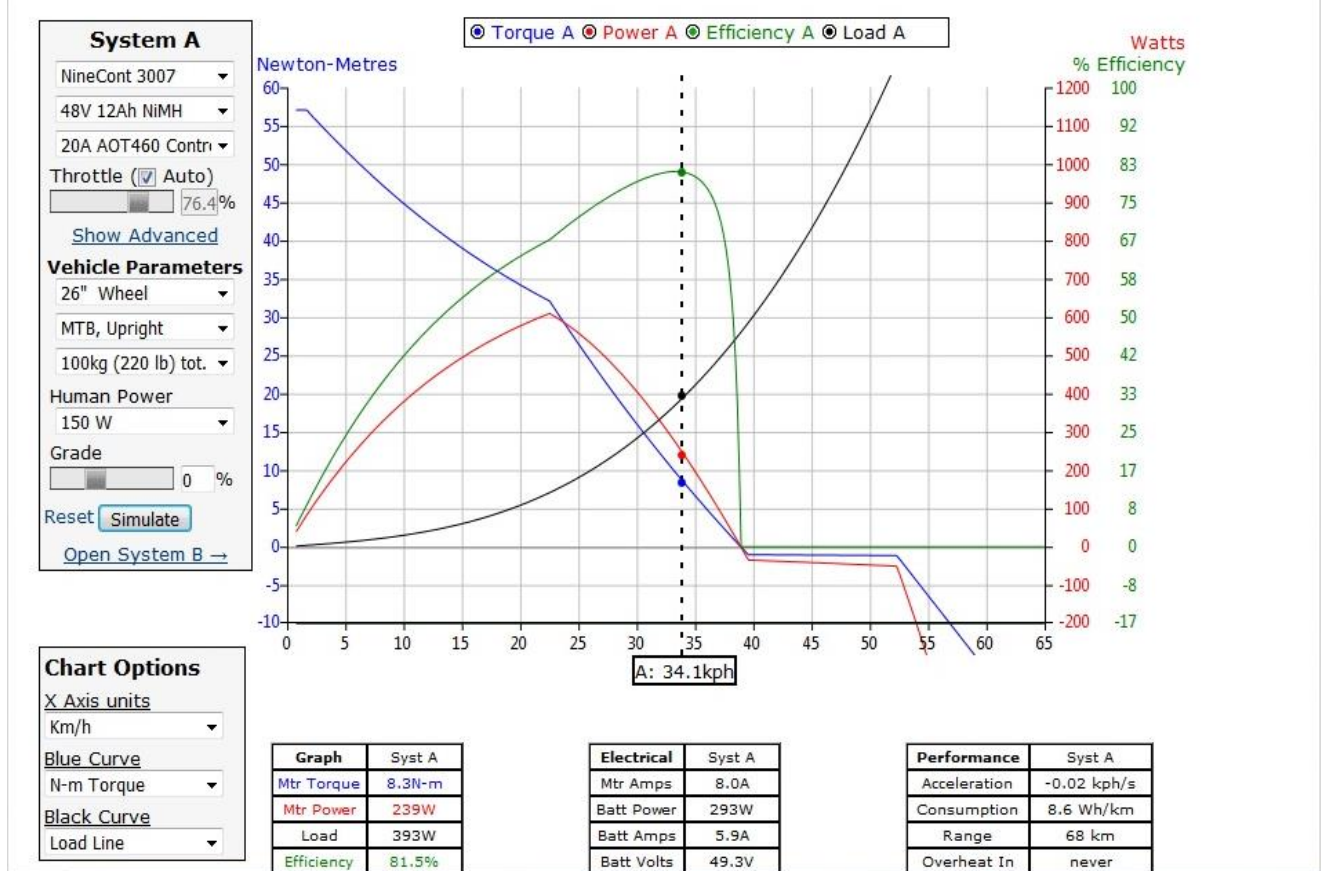


Figure-9 Simulation results [16]

Simulation Details are explained down below. The simulator was based on the following circuit model illustrated in Figure-10 for a battery powered permanent magnet motor and controller setup:

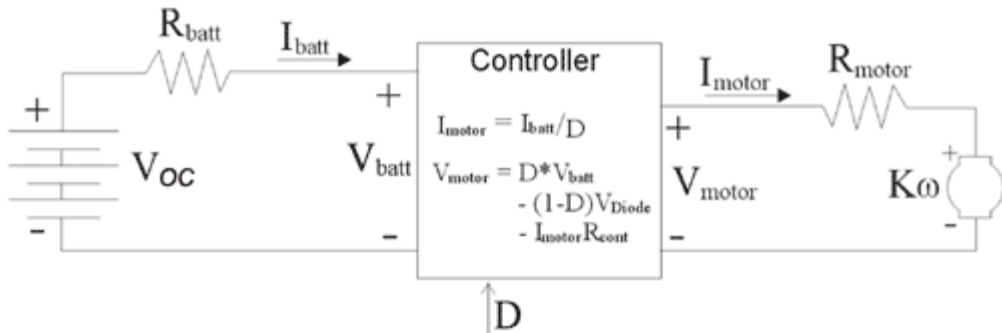


Figure-10 Simulation parameters of drivetrain [16]

- V_{oc} Is the open circuit battery voltage.
- R_{batt} Is the first order internal resistance of the battery.
- I_{batt} Is the current draw from the battery pack.

- D is the PWM duty cycle, which can range from zero to one. This value is generally equal to the throttle setting, but that can be ridden to keep I_{batt} the specified current limit.
- I_{Motor} is the current through the motor windings.
- R_{Motor} is the winding resistance of the motor.
- K is the motor constant, in Nm/A or V/(Rad/sec).
- w is the wheel speed in radians per second.

The controller is assumed to be a single quadrant (non-regen) controller, with the indicated input and output equations.

The actual model in Simulator is substantially taking into account the commutations that happen on a regular basis as a function of the speed and number of poles of the hub motor, and determining the resulting current waveforms that are produced when this is applied to the inductive motor windings.

$$Torque = I_{motor} * K - (A_0 + A_1w + A_2w^2) \quad (2.6)^3$$

The power is calculated simply as this output torque times motor angular speed:

$$Power = Torque * w \quad (2.7)^3$$

The efficiency is calculated from the useful power output divided by the total electrical power consumed (it does not take into account the losses internal to the battery pack):

$$Efficiency = \frac{Power}{(V_{oc} - R_{batt} * I_{batt})I_{batt}} \quad (2.8)^3$$

The controller is assumed to be a single quadrant (non-regen) controller, with the indicated input and output equations.

The parameter values that are chosen for the motor model are based on directly measured data. Original dynamo setup are pictured for simulation above in Figure-11.

The maximum speed values that can be achieved at different slopes during driving on a road with a power output of 250 W in accordance with EN 15194 and a speed not exceeding 25 km/h.

In high-performance electric bicycles, the Hub-BLDC direct current motor is commonly used. For this reason, the characteristics of the brushless direct current motor will be examined in detail and the most appropriate motor structure will be selected for the basic needs of the electric

³ Larminie, J., ve Lowry, J. (Authors) (2003). *Electric Vehicle Technology Explained*, John Wiley & Sons Ltd.

bicycle. A brushless direct current motor (BLDC) is an electric motor in the class of synchronous motors which, unlike conventional motors, does not have an excitation winding or brush collector system. Permanent magnets form a long lasting magnetic field on the rotor; in the stator, there are field windings. The commutation operation is performed electronically via a power electronic circuit. Structurally, it is similar to a synchronous motor with a permanent magnet in the rotor, but in terms of performance, it carries classical direct current motor characteristics. As with the direct current motor, the induced voltage is the trapezoidal wave and is ideally driven by rectangular pulse currents [17].

Today, along with improvements in materials and production technology, the magnetic field intensities of permanent magnets are increasing and their use in electric motors is becoming widespread. Various permanent magnet materials such as AlNiCo, ferrite, SmCo, NdFeB are widely used for electric motors. Although AlNiCo magnets provide advantages of high flux density and Curie temperature, they also limit magnet placement due to the low coercive value. Ferrite magnets can withstand high temperatures due to their ceramic structure. In addition, they are often preferred for low cost motor production because of their low cost and durability. On the other hand, AlNiCo and NdFeB (neodymium) magnets, which are rare earth elements, are expensive materials, but they are preferred in applications where high performance is required because they can provide high flux density and field strength [18].

Demagnetization in the brushless direct current motor is due to the effect of the magnetic field generated by the current flowing through the stator windings. This magnetic field generated by stator has direct effects on the life span of the magnets. The demagnetization curves of the magnet materials are given in comparative Figure-12 [18].

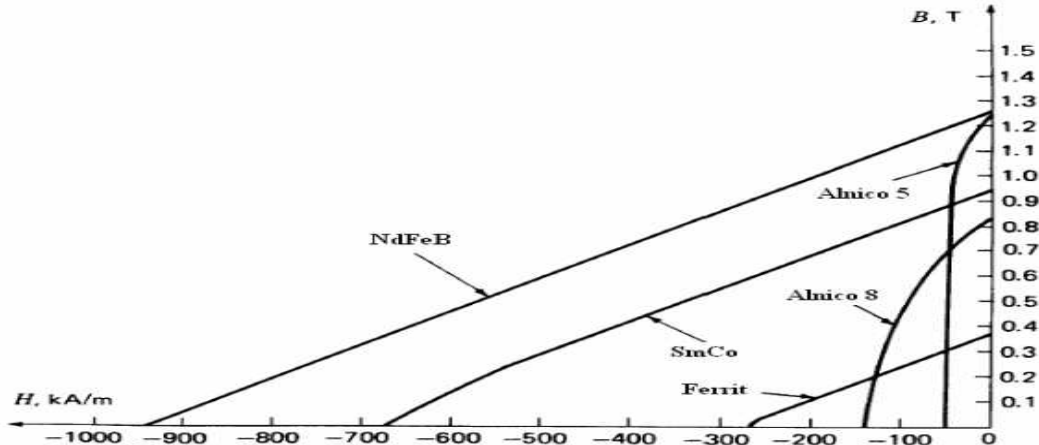


Figure-12 Demagnetization curves of various permanent magnet materials [19]

Brushless DC motors are produced from rotor and stator ferromagnetic materials. The optimum number of poles is a complex function of motor geometry and material properties [20].

When the relationship between the electrical frequency of the motor and the mechanical rotation speed of the magnetic field, i.e., the synchronous speed, is examined it is seen that the number of poles ($2p$) and the rotation speed of the motor N_m (in rpm) are inversely proportional.

For this reason, high-speed motors are generally manufactured with 2 to 4 poles, while pole numbers must be chosen high for the motor to be used in applications requiring low speed and high torque [20].

$$N_m = 120F_e/2p \quad (2.9)$$

High pole motors have low active weights. The active weight can be expressed as the weight of the components contributing to the torque production of the motor: the back yoke, stator plates, windings and permanent magnets.[21].

The stator core is manufactured by pressing laminated silicon steel sheets with a thickness of 0.3-0.5 mm in order to reduce the circulation current and the slots on which the conductors are placed are opened. Windings can be concentrated or can be manufactured as distributed coils.

The number of stator slots is determined by the rotor poles, the number of phases and the winding shape. Although the BLDC motors can be produced in several phase numbers, the power electronics controlling the phase currents are designed as two or three phases in order to keep the number of elements low. Phase windings each of which is of equal length are mostly delta connected [22].

Electric motors can be produced in a wide variety of structures.

Choosing the motor type and power

Observing the results from simulations on Figure-9 the minimum power required come above of all frictions is approximately 100W. To starter, due to low budget limitations it was decided to use two BLDC motor with each of them with 180W. This offers approximately 260W of traction power.

Due to the analysis, the motors may be mounted in the front wheel using 3D printed parts that will be designed later.

CHAPTER 3

Brushless Electric Motors (BLDC)

In this section, it is made a short survey to the types of BLDC motors trying to explain the differences and see the advantage and disadvantage in order to choose the best motor type for an electric bicycle.

Permanent magnet BLDC motors

The advancement in technology and development of modern control techniques using solid-state switching devices and microelectronics have contributed to new energy efficient electric drives, which are able to overcome limitations such as low power factor and nonlinear speed torque characteristics and satisfy the requirements of a variable speed drive. The permanent magnet machines have the features of high torque to size ratio and possess very good dynamic characteristics due to low inertia in the permanent magnet rotor, a better power factor and better output power per unit mass / volume without losing the reliability [23].

Permanent magnet brushless DC motor (PMBLDC) motors are increasingly being used in a wide spectrum of applications such as domestic equipment, automobiles, information technology equipment, industries, public life appliances, transportation, aerospace, defense equipment, power tools, toys, vision and sound equipment and medical and health care equipment ranging from microwatts to megawatts. This has become possible because of their superior performance in terms of high efficiency, fast response, lightweight, precise and accurate control, high reliability, maintenance free operation, brushless construction, high power density and reduced size.

Recent developments in PMBLDC motor technology are in terms of availability of high performance rare earth PM materials, varying motor constructions such as axial field, radial field, package type, rectangular fed, sine fed motors, improved sensor technology, faster response semiconductors modules. Low cost high performance microelectronics devices, new control philosophy such as robust, adaptive, fuzzy, neural AI based controllers, have led to their widespread use in the large speed ranges from few revolutions to thousand revolutions per minute (rpm). They have been proven most suitable for position control in machine tools, robotics.

Types of brushless motors

There are two types of BLDC motors which are called the in-runner and out-runner. The in-runner motor has permanent magnets located on the inside of the stationary electromagnets. An out-runner motor has the permanent magnets located on the outside.

In-Runner motors

In-runner motors are good when high speeds are needed. They are more efficient than out-runner motors the faster they spin. However, due to the gearbox, it makes the motor more susceptible to parts failing [17]. Its main characteristics are:

- High RPM's, low torque
- More efficient than out runners due to the higher rotation speed
- Require a gearbox
- Wide prop selection for Aircraft Applications
- Noisy

Out-Runner motors

Out-runner motors spin slower but output more torque. They are easier to use since a gearbox is not required and run very quietly [17].

The characteristics of out-runner motors are:

- Low RPM's, high torque
- Less efficient than in runners
- No gearbox required
- Silent

In the in-runner rotor motors, heat transfer is easy due to the presence of windings and the presence of an internal rotating part, but winding is difficult. The rotor inertia must be low, moment / inertia ratio should be high. In runner and out runner motor types are shown in Figure-13.

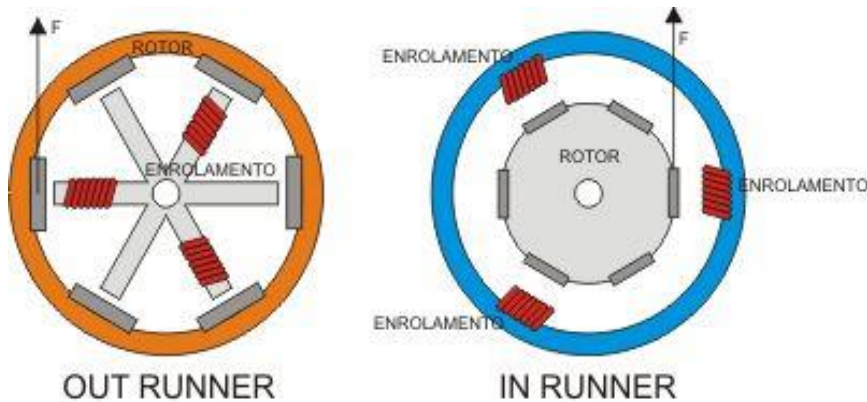


Figure-13 In-runner and out runner types [17]

It is preferable to use inner rotor motors to keep the rotor radius small because the inertia is proportional to the radius in such servo applications. In order to reduce the inertia, it is necessary to reduce the size of the magnets. In such applications, high energy density magnets are preferred depending on the performance/cost ratio.

Instead of using expensive neodymium magnets, low cost ferrite magnets can be used in applications where high flux density is not required. External rotor motors are designed with a larger air gap than internal rotor motors.

The cost of disk type motors is low. However, since there is a large air gap in these types of motors, too much loss can be seen in the magnetic flux. In applications with a speed as high as 1000 rpm, heat problems arise in the stator and rotor disc quadrants [17].

Rotor placement of magnets can be accomplished with different designs, surface mount or embedded magnet. The surface magnet structure is used in low speed applications because of the risk of disintegration of the magnets. In high-speed applications, the embedded (inset) magnet rotor structure is used to remove this disadvantage.

For brushless direct current motors to produce a continuous and uniform moment, the current flowing through the armature windings must be in the same direction as the pole current. Depending on the rotor position, the relevant phase should be fed with a square wave current in regions where the induced trapezoidal voltages are flat [17].

In brushless motors, the system must be fed with the correct voltage since the electronic commutation is carried out via an inverter. Encoder, resolver and Hall sensors are used for position detection. In addition, there are studies to realize the sensor processing without sensor. The back EMF detection method that occurs in the motor windings was used during the execution of the sensorless motion control.

CHAPTER 4

Brushless DC (BLDC) motors and sensorless drives

The brushless dc motor is one of the permanent magnet synchronous motor, having permanent magnets on the rotor and trapezoidal shape back EMF. The BLDC motor employs a dc power supply switched to the stator phase windings of the motor by power devices, the switching sequence being determined from the rotor position.

The phase current of BLDC motor, presents typically a rectangular shape, and is synchronized with the back EMF to produce constant torque at a constant speed. Electronic transistors, which supply current to the motor windings as a function of the rotor position, replace the mechanical commutator of the brush dc motor. This kind of ac motor is known as brushless dc motor, since its performance is similar to the traditional dc motor with commutators.

These brushless dc motors are generally driven by using a three-phase inverter, requiring a rotor position sensor for starting and for providing the proper commutation sequence to control the inverter. These position sensors can be Hall sensors, resolvers, or absolute position sensors. A typical position sensor used in motor control systems for BLDC is the Hall sensor. Those sensors will increase the cost and the size of the motor only if the motor is very small, and special mechanical arrangement needs to be made for mounting the sensors in to the rotor. These sensors, particularly Hall sensors, are temperature sensitive, limiting the operation of the motor below about 75°C .

On the other hand, they could reduce the system reliability because of the components and wiring. In some applications, it even may not be possible to mount any position sensor on the motor. Typically, to drive a BLDC motor is used a three-phase inverter, which is also called a six-step commutation drive, therefore sensorless control of BLDC motor has been receiving great interest in this decade specially in applications like drones or car fuel pumps.

Typically, a three-phase inverter with, also called, six-step commutation drives a BLDC motor. The electronically controlled conducting interval for each phase is 120° . The commutation phase sequence is like AB-AC-BC-BA-CA-CB as seen in Figure-14.

Each conducting stage is called one-step. Therefore, only two phases conduct current at one time, leaving the third phase floating. In order to produce maximum torque, the inverter should be commutated every 60° so that current is in phase with the back EMF.

The commutation sequence is determined by the rotor position, which can be detected by Hall sensors or estimated from motor parameters, or the back EMF on the floating coil of the motor if it is a sensorless system.

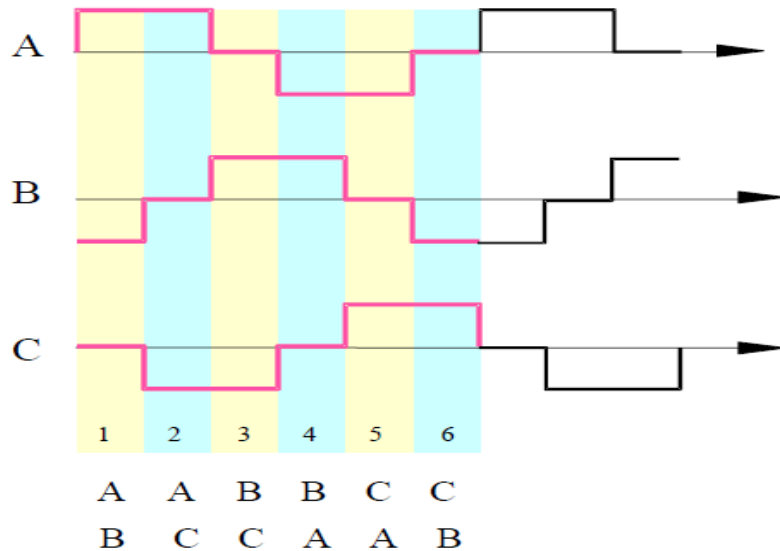


Figure-14 BLDC Motor driving sequence [22]

There are many types of position sensing using back EMF of the motor, and the one is position estimation using motor parameters, terminal voltages, and currents. The second type scheme usually needs DSP to do the complicated computation, and the cost of the system is relatively high. Therefore, the back EMF sensing type of sensorless scheme is the most commonly used method.

In brushless dc motor, only two out of three phases are excited at one time, leaving the third phase floating. The back EMF voltage in the floating phase can be measured to establish a switching sequence for commutation of power devices in the three-phase inverter [24].

K. Uzuka [22] originally proposed the method of sensing back EMF (will be referred as conventional back EMF detection method) to make a virtual neutral point that will, in theory, be at the same potential as the center of a Y wound motor and then to sense the difference between the virtual neutral and the voltage at the floating terminal.

However, when using a chopping drive, the neutral is not a standstill point. The neutral potential is jumping from zero up to near dc bus voltage, creating large common mode voltage since the neutral is the reference point. Meanwhile, the PWM signal is superimposed on the neutral voltage as well, inducing a large amount of electrical noise from switching high current on the sensed signal. To sense the back EMF properly, it requires a lot of attenuation and filtering. The attenuation is required to bring the signal down to the allowable common mode range of the sensing circuit, and the low pass filtering is to smooth the high switching frequency noise.

Filtering causes unwanted delay in the signal. The result is a poor signal to noise ratio of a very small signal, especially at start-up where it is needed most. Consequently, this method tends to have a narrow speed range and slow speed start up characteristics. To reduce the switching noise, the back EMF integration [25] and third harmonic voltage integration were introduced [26].

The integration approach has the advantage of reduced switching noise sensitivity. However, they still have the problem of high common voltage in the neutral. An indirect sensing of zero crossing of phase back EMF by detecting conducting state of freewheeling diodes in the unexcited phase was presented [27].

The implementation of this method is complicated and costly, while its low speed operation is still a problem. This report proposed an idea of a back EMF detection method, which does not require the motor neutral voltage. The true back EMF can be detected directly from terminal voltage by properly choosing the PWM and sensing strategy. The PWM signals are only applied to high side switches and the back EMF is detected during PWM off time. The resulting feedback signal is not attenuated, filtered, or reduced providing a timely signal with a very good signal/noise ratio. As a result, this sensorless BLDC driver can provide a much wider speed range, from start-up to full speed, than the conventional approaches mentioned above.

In the past, several integrated circuits based on neutral voltage construction have been commercialized [28] [29].

Unfortunately, all these ICs are all analog devices, which lack flexibility in applications, regardless of poor performance at low speed. DSPs can apply very complicated control theory and speed estimation for the sensor less BLDC motor control. However, the cost of DSP is still relatively high. 8-bit microcontrollers have been the mainstay of embedded control systems for a long time. The devices are available for a low cost; and the instruction sets are easy to use. Low system cost and high flexibility are good motivations to design a new microcontroller, which is dedicated to sensorless BLDC drive. As a result, a low cost mixed signal microcontroller applications is developed.

Open loop control

In open loop control mode, the input speed reference signal is directly translated into a PWM duty cycle value. This is then used by the commutation logic to drive the inverter bridge. The Hall Effect feedback signal is only used to perform the electronic commutation steps required to drive the motor. There is no real speed reading feedback. The motor stabilizes at a speed where the torque provided by the PWM duty cycle matches the load on the motor due to the sensor feedback. Open loop control mode is typically used by sensorless BLDC systems during start up until the rotor locks into rotation and can provide sufficient BEMF for positional feedback. A diagram for open loop control is represented in Figure-15 [30].

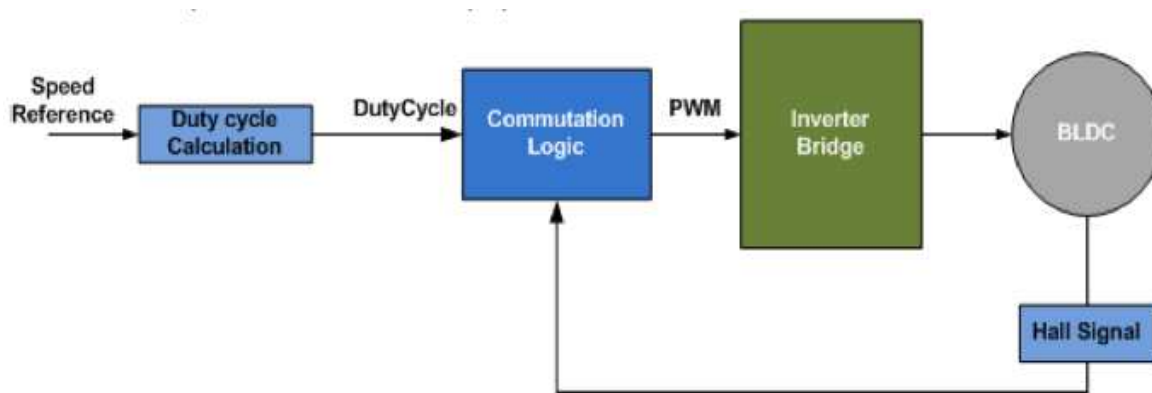


Figure-15 Open loop control block diagram [30]

Closed loop control

In closed loop control, a controller calculates the PWM duty cycle by measuring the actual motor velocity and comparing it with the desired velocity set by the speed reference. In the block diagram on, system shown in the Figure-16 below, the Hall Effect sensor signal is used to both drive the commutation logic and calculate the motor speed. The actual speed is compared with the speed reference, and the error value is fed into a PI controller.

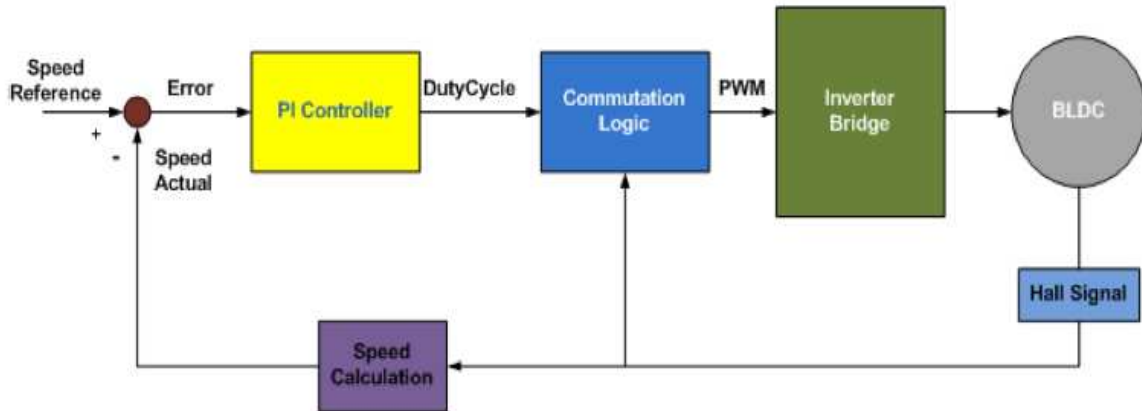


Figure-16 Closed loop control block diagram [30]

The PI controller modifies the error signal using proportional and integral gain constants to generate the PWM duty cycle. See in Figure-17.

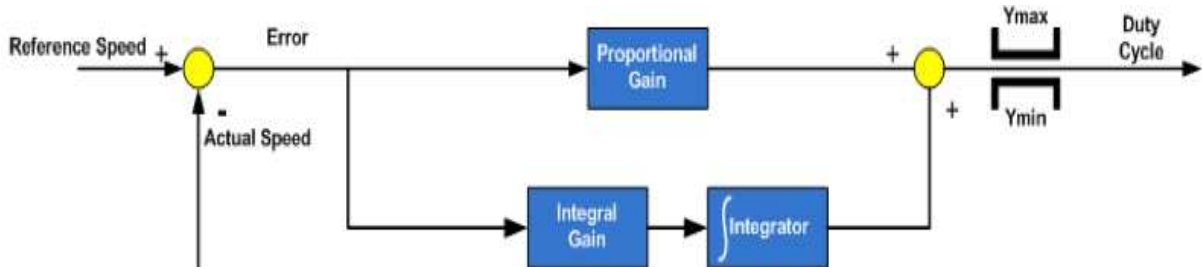


Figure 13 · Proportional-Integral Controller

Figure-17 PI controller block diagram [30]

$$(DutyCycle) = K_p * error + K_i * \int error dt \quad (4.1)$$

where K_p is the proportional gain, K_i is the integral gain, and error is the difference between the set and measured speed values.

As most calculations are done with digital microcontrollers, the following discrete time domain representation is more useful.

$$y_n(k + 1) = y_n(k) + K_l * e(k)$$

$$Y_n(k + 1) = y_n(k + 1) + K_p * e(k) \quad (4.2)$$

where $y_n(k + 1)$ is the current integrator term, $y_n(k)$ is the previous integrator term, $e(k)$ is the difference in reference speed and actual speed, and $y_n(k + 1)$ is the current computed duty cycle [36].

Sensorless BLDC motor driving systems

In this chapter, a brief review of the conventional back EMF detection will be mentioned first. Then, the back EMF detection will be described deeply. We will see the advantages of the back EMF sensing scheme and the sensorless system. Specially, a low cost mixed-signal microcontroller that is the most commercial and famous one dedicated for sensorless BLDC drives is developed, integrating the detection circuit and motor control peripherals with the standard 8-bit Atmega328 core.

Types of back EMF detection schemes

A three-phase BLDC motor, typically, is driven with six-step 120-degree driving mode. At one time instant, only two out of three phases are conducting current. For example, when phase A and phase B conduct current, phase C is floating. This conducting interval lasts 60 electrical degrees, which is called one-step. A transition from one-step to another different step is called commutation. So totally, there are six steps in one cycle.

As shown in Figure-14 in previous chapter, the first step is AB, then to AC, to BC, to BA, to CA, to CB and then just repeats this pattern. Usually, the current is commutated in such way that the current is in phase with the phase back EMF to get the optimal control and maximum torque/ampere. The commutation time is determined by the rotor position. Since the shape of back EMF indicates the rotor position, it is possible to determine the commutation timing if the back EMF is known. In Figure-18, the phase current is in phase with the phase back EMF. If the zero crossing of the phase back EMF can be measured, we will know when to commutate the current [31].

As mentioned before, at one time instant, since only two phases are conducting current, the third winding is open. This opens a window to detect the back EMF in the floating winding. The concept detection scheme can be seen in Figure-29 [32].

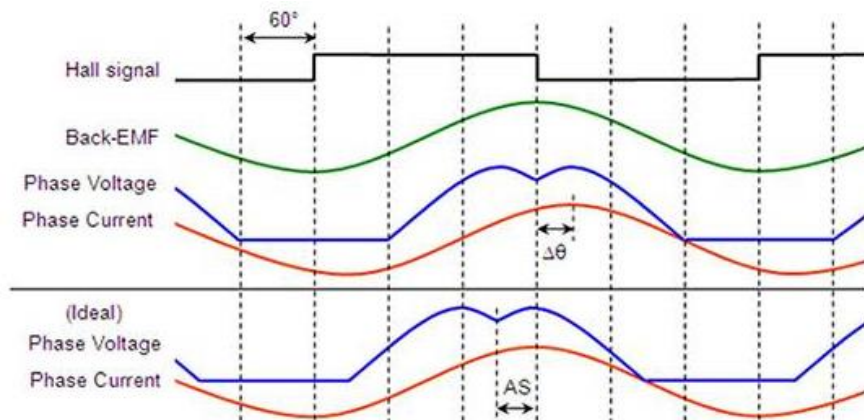


Figure-18 The phase current is in phase with the back EMF in BLDC motor [32]

The terminal voltage of the floating winding is measured. This scheme needs the motor neutral point voltage to get the zero crossing of the back EMF, since the back EMF voltage is referred to the motor neutral point. The terminal voltage is compared to the neutral point, and then the zero crossing of the back EMF can be obtained. In most cases, the motor neutral point is not available. In practice, the most commonly used method is to make a virtual neutral point that will, in theory, be at the same potential as the center of a Y wound motor and then to sense the difference between the virtual neutral and the voltage at the floating terminal. Resistors build the virtual neutral point, which are shown in Figure-19.

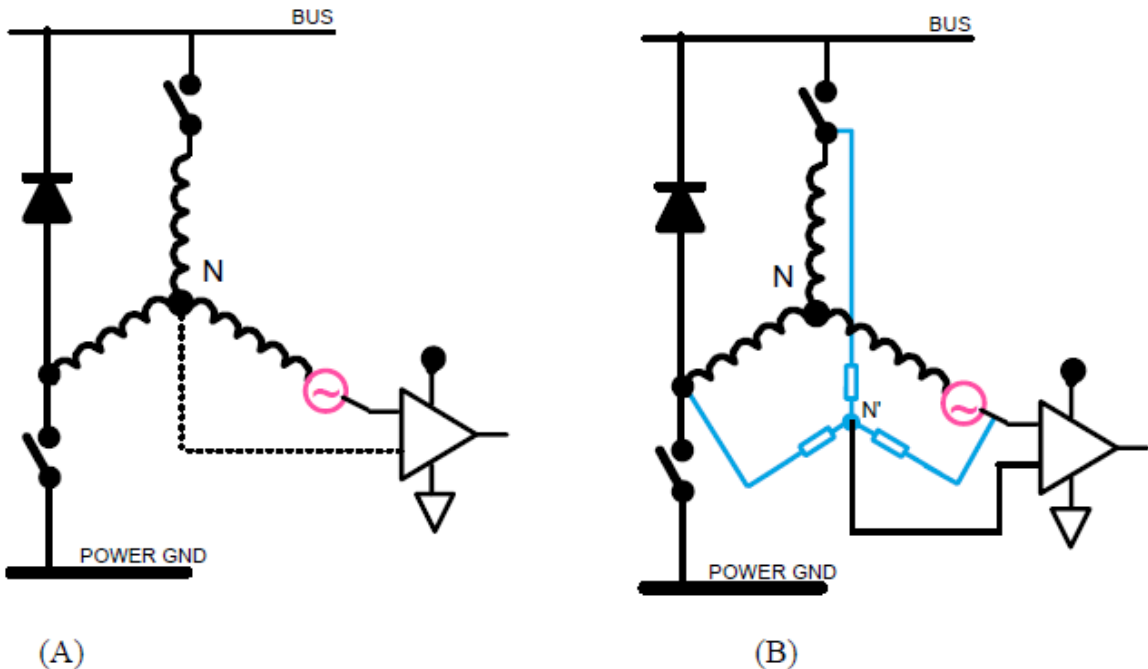


Figure-19 (A) Back EMF zero crossing detection scheme with the motor neutral point (B) back EMF zero crossing detection scheme with the virtual neutral point.

Because of the PWM drive, the neutral point is not a standstill point. The potential of this point is all the time jumping up and down. It generates very high common mode voltage and high frequency noise. Therefore, we need voltage dividers or low pass filters to reduce the common mode voltage and smooth the high frequency noise, shown in Figure-19 for instance, if the dc bus voltage is 300 V, the potential of the neutral point can vary from zero to 300 V. The allowable common mode voltage for a comparator is typically a few volts, like 5V or 3.3V. We will know how much attenuation should be. Obviously, the voltage divider will reduce the signal sensitivity at low speed, especially at start up where it is needed most. On the other hand, if we build a low pass filter will induce a fixed delay independent of rotor speed. As the rotor speed increases, the percentage contribution of the delay to the overall period increases. This delay will disturb current alignment with the back EMF and will cause severe problems for commutation at high speed. Consequently, this method tends to have a narrow speed range.

In the past, there have been several integrated circuits, which enabled sensorless operation of the BLDC, based on the scheme described above. These included Arduino Atmega328p. The back EMF integration approach has the advantage of reduced switching noise sensitivity and perform automatic adjustments of the inverter switching instants according to changes in the rotor speed [22].

The back EMF integration still has accuracy problems at low speeds. The rotor position can be determined based on the stator third harmonic voltage component [33].

The main disadvantage is the relatively low value of the third harmonic voltage at low speed.

In [34], the rotor position information is determined based on the conducting state of freewheeling diodes in the unexcited phase. The sensing circuit is relatively complicated and low speed operation is still a problem.

Direct Back EMF Detection using an ADC input

As described before, the noisy motor neutral point causes problems for the sensorless system. The back EMF detection is trying to avoid the neutral point voltage. If the proper PWM strategy was selected, the back EMF voltage referred to ground can be extracted directly from the motor terminal voltage. The circuit of the connection to an Atmega328p ADC description can be seen in Figure-20. The PWM drive signal can be arranged in three ways:

- On the high side: a high frequency PWM is applied only on the high side switch, the low side is on during the low frequency PWM that make a 60° step.(see Figure-22 for proper understanding of the what means high and step PWM signal explained later in PWM technique and Current Chopping subsections)
- On the low side: the PWM is applied on the low side switch, the high side is on during the step.
- On both sides: the high side and low side are switched on/off together.

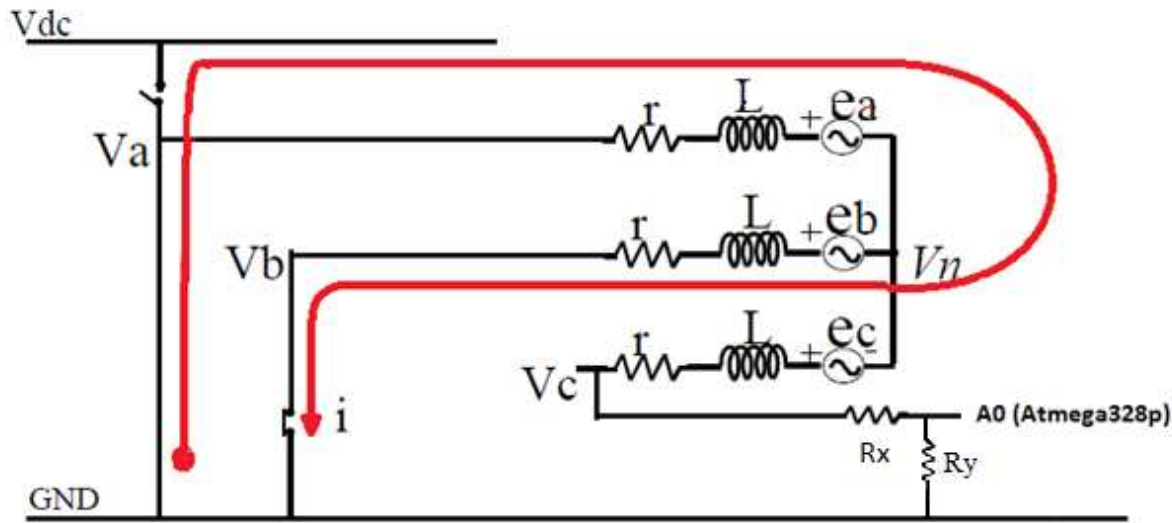


Figure-20 Circuit model of BLDC motor

When the upper switch of phase A has turned on, the current is flowing through the switch to winding A and B. When the upper transistor of the half bridge is turned off, the current freewheels through the diode paralleled with the bottom switch of phase A.

During this freewheeling period, the terminal voltage V_c is detected as Phase C back EMF when there is no current in phase C.

From the circuit, it is easy to see $V_c = e_c + V_n$, where V_c is the terminal voltage of the floating phase C, e_c is the phase back EMF and V_n is the neutral voltage of the motor.

From phase A, if the forward voltage drop of the diode is ignored, we have:

$$V_n = 0 - r_i - L \frac{di}{dt} - e_a \quad (4.3)$$

From phase B, if the voltage drop on the switch is ignored, we have:

$$v_n = r_i + L \frac{di}{dt} - e_b \quad (4.4)$$

Adding (4.1) and (4.2), we get:

$$V_n = \frac{V_{dc}}{2} - \frac{e_a + e_b}{2} \quad (4.5)$$

Assuming a balanced three-phase system, if we ignore the third harmonics, we have

$$e_a + e_b + e_c = 0 \quad (4.6)$$

Or, if we don't ignore the third harmonics, we will have

$$e_a + e_b + e_c = e_3 \quad (4.7)$$

where e_3 is the third harmonics.

Let us first finish the analysis without considering the third harmonics. From (4.3) and (4.4),

$$V_n = \frac{e_c}{2} \quad (4.8)$$

So, the terminal voltage V_n ,

$$V_n = e_c + V_n = \frac{3}{2} * e_c + \frac{V_{dc}}{2} \quad (4.9)$$

From the above equations, it can be seen that during the off time of the PWM, which is the current freewheeling period, the terminal voltage of the floating phase is directly proportional to the back EMF voltage without any superimposed switching noise. It is also important to note that this terminal voltage is referred to the ground instead of the floating neutral point.

Therefore, the neutral point voltage information is not needed to detect the back EMF zero crossing, and we do not need to worry about the common mode voltage. Since the true back EMF has extracted from the motor terminal voltage, the zero crossing back EMF can be detected very precisely.

As a summary, main advantages and disadvantages of the back EMF sensing technique over the conventional schemes as shown in Figure-20 can be listed as following:

1. It has less sensitivity first, since it uses a voltage divider, there is a lot of attenuation. That is why we do not have good SNR at low speed operation. Second, the high frequency switching noise is also attenuated because the back EMF is sampled during the PWM off time. Since we do not have a synchronous sample rate, sampling cannot compensate of the switching noise.
2. The back EMF is taken as an instant value due to no filtering in the circuit, which will be suitable for high-speed operation.
3. This sensing technique can be easily used to either high voltage or low voltage systems without much effort to scale the voltage.
4. Fast motor start-up is not possible due to the precise back EMF zero crossing detection without attenuation.

PM-BLDC motor position detection sensored or sensorless

The sampling techniques have developed to detect the back EMF zero crossing. In last decade, with the development of IC mixed-signal technology, SOC (System On Chip) devices are feasible. Precision analog, high-throughput arm processors, in system programmable memory, and other peripherals can be integrated on a single chip.

SOC devices have many advantages, including lower system cost, reduced board space, and superior system performance and reliability. However, the SOC devices generally maintains the gate driver circuit and power MOSFET's in one small chip. As a disadvantage, the price is higher than other components.

The 8-bit microcontroller has been the mainstay of embedded-control systems for nearly 20 years. The devices are available for a low cost; instruction sets are easy to use. As a result, the back EMF detection circuit was used with a standard Atmega microcontroller to become a low cost dedicated sensorless BLDC microcontroller.

Detecting motor angular position with Hall Effect sensors

To control an e-bike motor the controller needs to know the angular position of the motor at every point in time so that it can keep pushing it around. It gets out the motor position from the signals coming back from the hall sensors a detailed description can be seen in Figure-21.

When the signal from the Hall sensor is high that means that one of the motor magnets is going right past it, when the signal is low that means the motor magnet has already gone past.

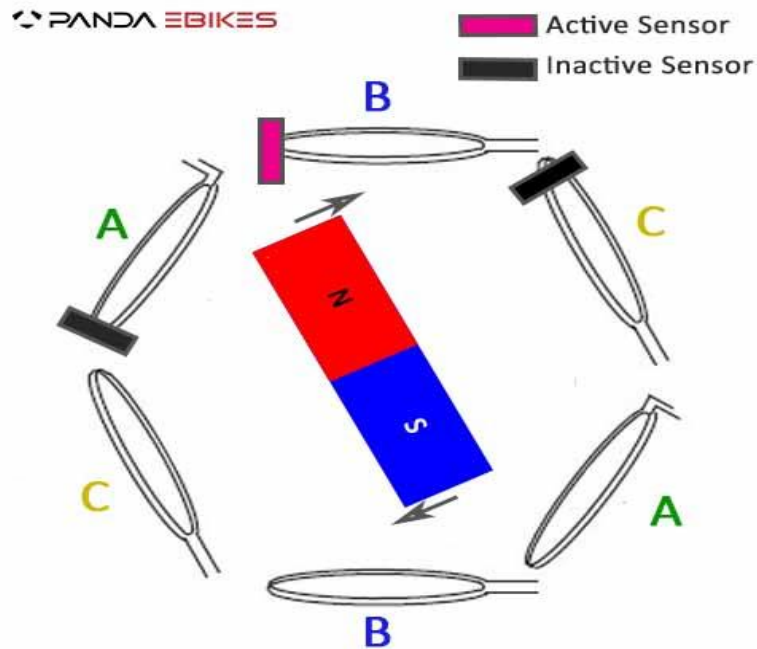


Figure-21 Hall Effect sensors in hub motor [35]

The working principle of Hall Sensor is when electric current flows through a material, electrons move through it in pretty much a straight line. Put the material in a magnetic field and the electrons inside it are in the field too. A force acts on them (the Lorentz force) and makes them deviate from their straight-line path. Now, the electrons in this example would bend as from their point of view, from left to right. With more electrons on the right side of the material than on the left, there would be a difference in potential (a voltage) between the two sides. The size of this voltage is directly proportional to the size of the electric current and the strength of the magnetic field [35].

In Chapter 6, sensored BLDC motors will be detailed in terms of sensor implementation.

Detecting the back EMF strategies to improve back EMF Detection

Firstly, let us take a look on the implementation of the synchronous sampling of the back EMF zero crossing. For low voltage applications, the voltage drop across the BJT's or MOSFET's will affect the performance. When the motor speed goes low, zero crossing is not evenly distributed. Besides, if the speed goes further low, the back-EMF amplitude becomes too low to detect [38]. There are two methods to correct the offset voltage of back EMF signal. One is the PWM technique another one is the Current Chopping [36].

PWM technique

One of them is to use PWM as shown in Figure-22, which also reduces the conduction loss [37]. PWM method is used to eliminate the effect of high current spikes until maximum throttle. PWM uses a constant threshold current value for avoiding flowing overcurrent to each phase of BLDC motors [38].

In order to keep the current at a threshold value a controller must sense the current flowing to each phase. Moreover, when the current reach the threshold value the controller must keep switching the corresponding MOSFET to keep the current at the threshold value.

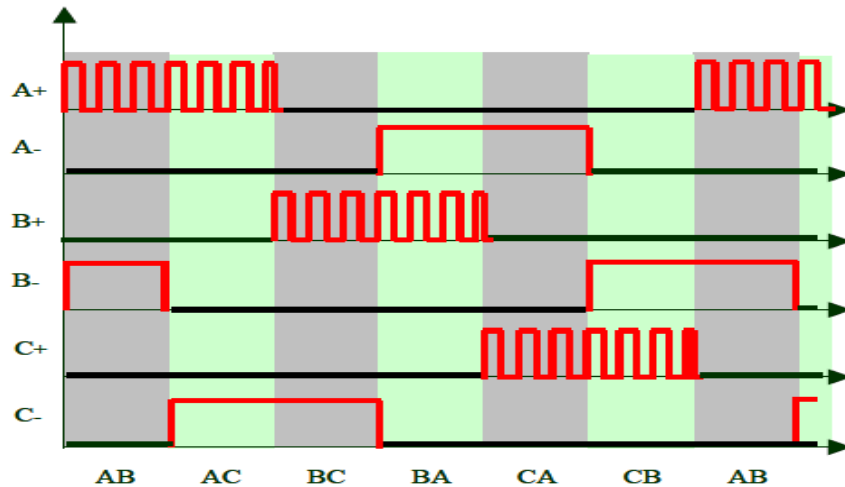


Figure-22 PWM Algorithm [38]

However, at low speed especially during the start-up, the back-EMF itself is very small, and the second term will play a significant role. This voltage offset will cause unevenly distributed back EMF zero crossings, which causes unexpected commutation and will affect the performance of the system. In addition, because the back-EMF signal is too weak at low speed, an amplifier can be used as a pre-conditioning circuit for adjusting the offset and amplifying the signal near the zero crossing [39].

Chopping current control

One difficulty with stepper motor operation is that the time constant (L/R) of the motor windings prevents current from increasing rapidly during pulses. This means that unless the voltage is very high, the current can never reach its full rated value, especially when the pulse rate is high (i.e. at high motor speeds). In order to get high current – and therefore high torque at high speeds, the voltage needs to be kept as high as possible and the inductance as low as possible. Nevertheless, in traditional L/R drives, the voltage must be kept low in order to keep the steady state current from becoming excessive.

A chopper drive addresses the problem of obtaining high torque at high speed from a BLDC motor by turning the output voltage to the motor on and off rapidly to control the motor current. At each step of the motor, a very high voltage (typically eight times higher than the motor's nominal voltage) is applied to the motor windings. This causes the current to rise rapidly,

according to the relationship between current rise and inductance. It also allows higher current to be produced, according to Ohm's law.

A current sensing resistor placed in series with each phase winding regulates current in a chopper drive. As current increases, voltage develops across the resistor, and a comparator monitors this voltage level. At a predetermined reference voltage, the output voltage is turned off (chopped) until the next pulse takes place. In this way, current builds and declines as the voltage switches off and on, resulting in the proper average current per step cycle. This enables precise control of torque, regardless of variations in the power supply voltage. It also gives the shortest possible time for current build-up and decline can see on Figure-23.

A constant, fixed frequency of current chopping typically 20 kHz or higher (above the audible range) varies the width of the output pulses. Winding impedance varies with motor speed, so at higher speeds (higher impedance in the windings) the current on time is longer, which produces a larger pulse width, allowing the current to build to the proper level. At lower speeds (lower winding impedance) the current on time is shorter, giving a smaller pulse width. This technique is also referred to as pulse width modulation (PWM) [38].

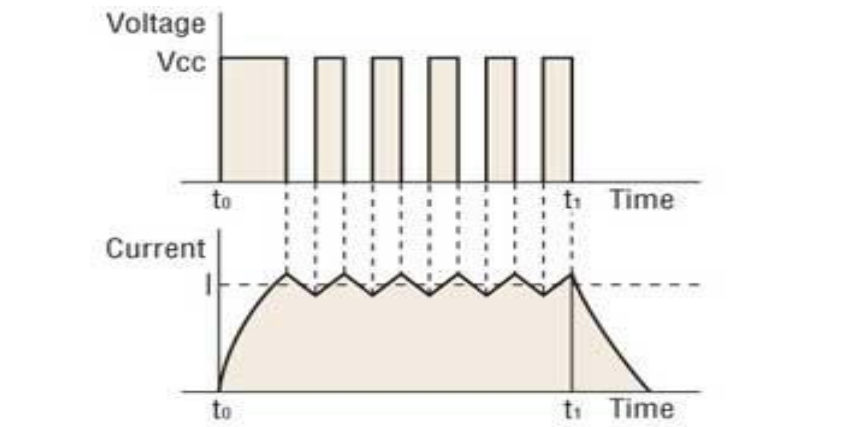


Figure-23 Current chopping technique [40]

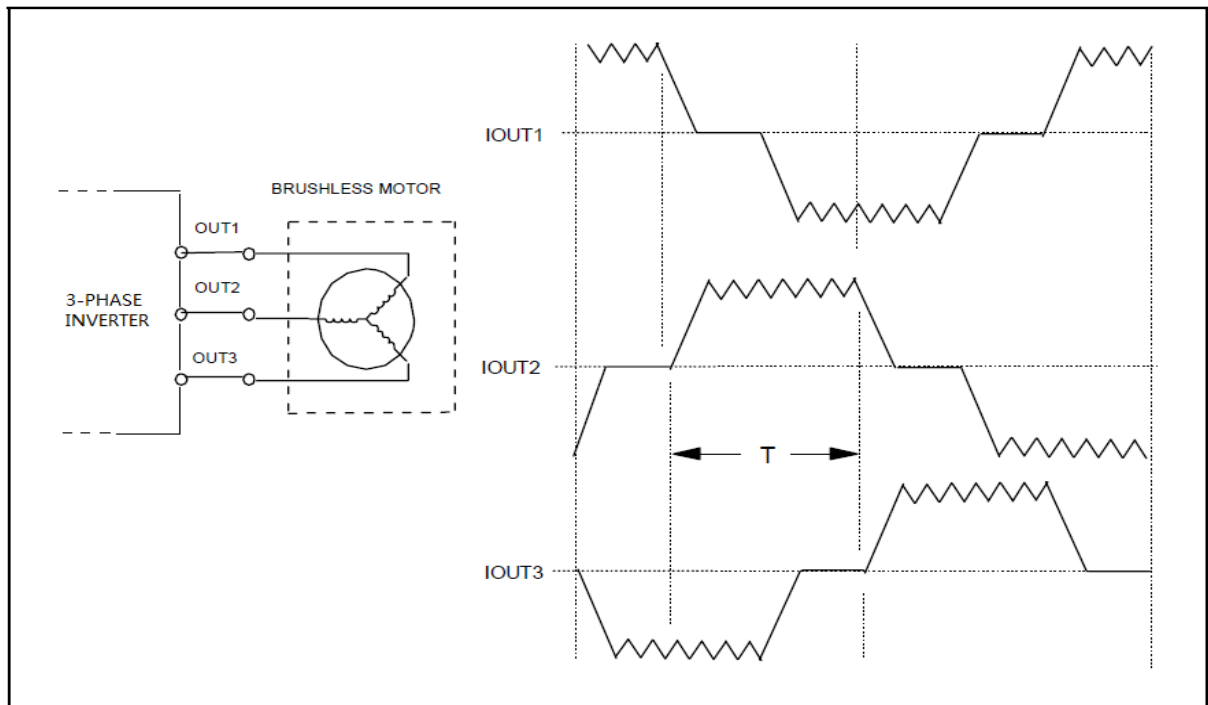


Figure-24 Three Phase Brushless motor control sequence with current chopping [41]

Conventional 120° PWM

This technique can be applied to a three-phase BLDC drive, and consists of a three-phase inverter and a BLDC motor. It can be controlled by the PWM technique to give proper commutations so that two of the three phases are with on states and the remaining one is with floating state. Moreover, the sequence of commutations has retained in proper order such that the inverter performs the functions of brush and commutator in a conventional DC motor, to generate a rotational stator flux. Figure-25 shows the PWM waveforms for this conventional approach [39], which has low switching losses in the inverter side at the cost of significantly high harmonic contents. These technic without current chopping feature will increase the current conception losses in the coil. Moreover, increasing the current conception will cause overheating problem on the coils of the motor.

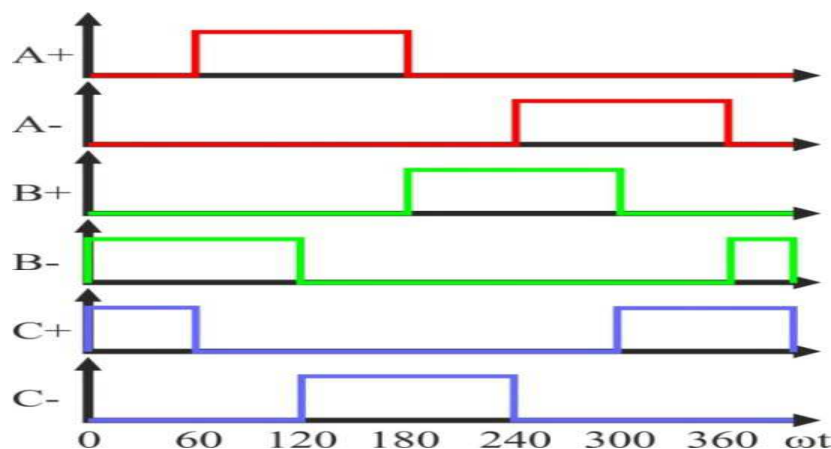


Figure-25 PWM Conventional 120° PWM [38]

Technique of virtual neutral point

In a typical inverter configuration, as Figure-26 illustrates, two phases are always conducting current and only one phase is available to measure back-EMF. To measure the back-EMF across a phase, the conventional method requires monitoring the phase terminal and the motor neutral point. The zero crossing of the back-EMF can be obtained by comparing the terminal voltage to the neutral point. In most cases, the motor neutral point is not available.

The most commonly used method is to build a virtual neutral point that will be theoretically at the same potential as the neutral point of the wye-wound motor [42].

The conventional detection scheme is quite simple and when a PWM signal is used to regulate motor speed or torque/current, the virtual neutral point fluctuates at the PWM frequency. As a result, there is a very high common-mode voltage and high frequency noise. Voltage dividers and low-pass filters, as shown in Figure-26, are required to reduce the common-mode voltage and minimize the high-frequency noise [42].

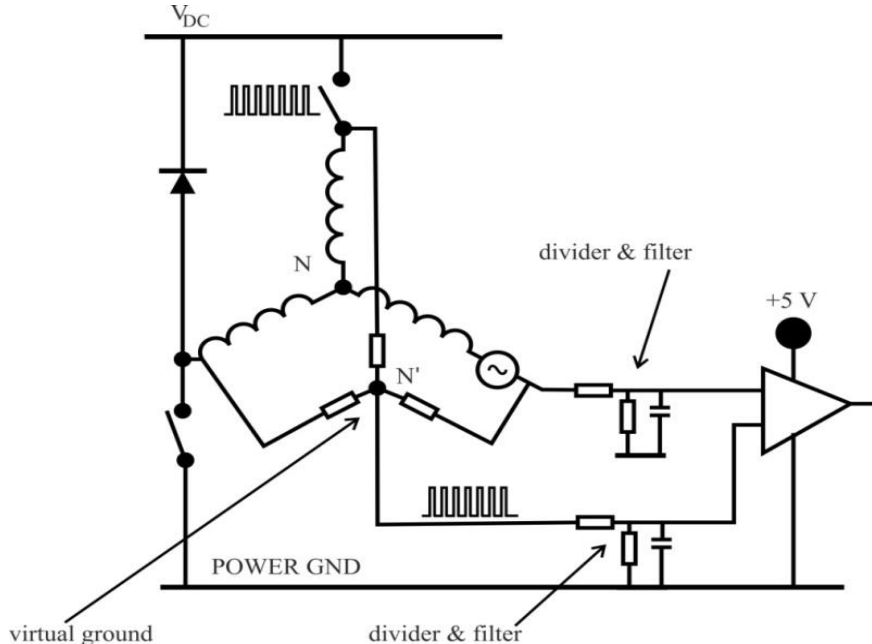


Figure-26 Back EMF detection with neutral point and LPF [42]

Other sensorless techniques estimation and Model-Based methods

It is convenient when designing feedback control systems, such as the motor position and speed, to assume initially that the entire state vector of the system to be controlled is available through measurement. If the entire state vector cannot be measured, as it is typical in most complex systems, the control law deduced cannot be implemented. Either thus, a new approach that directly accounts for the no availability of the entire state vector must be devised, or a suitable approximation to the state vector that can be substituted into the control law must be determined.

Several research works describe these advance methods and techniques listed below:

1. Sliding-Mode Observer (SMO) [39]
2. Direct Torque Control method (DTC) [43] [44] [46] [47]
3. Extended Kalman Filter (EKF) [48] [49]
4. Model Reference Adaptive System (MRAS) [50].
5. Adaptive observers [51]
6. Artificial Neural Networks (ANN) [52] [53].

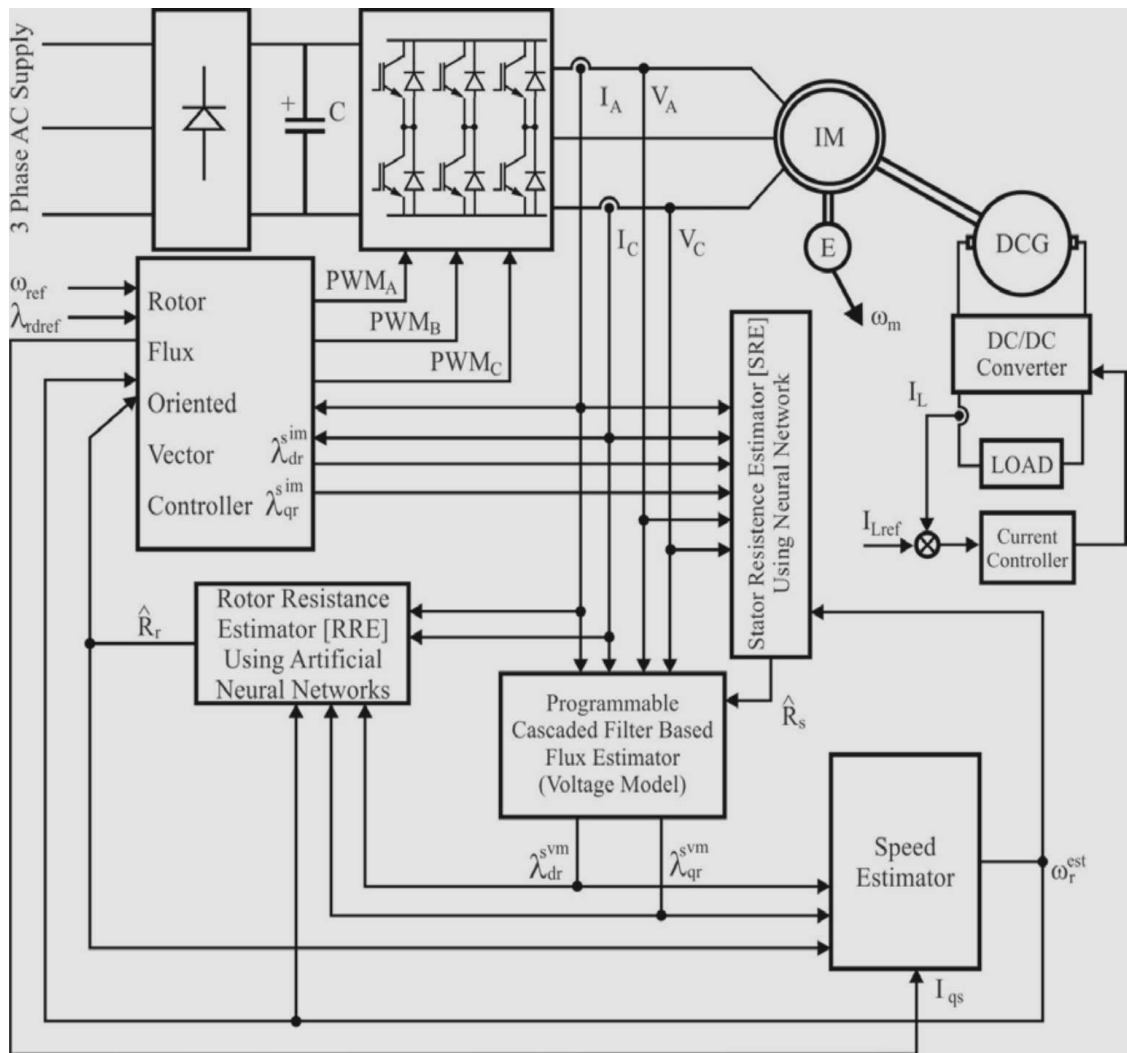


Figure-27 Example of advance techniques of ANN [53]

CHAPTER 5

Electric Bicycle Project Implementation

Purposed traction drive of this report

In this scope, it is aimed to design a lightweight and easy to implement drive system for electric bicycles with a high (power/weight) ratio. For these reasons it was decided to use a friction horizontal drive system. However due to the time and budget limitations and overheating problems for the motor there was no time to implement the purposed driving system depicted in Figure-28 to a bicycle.

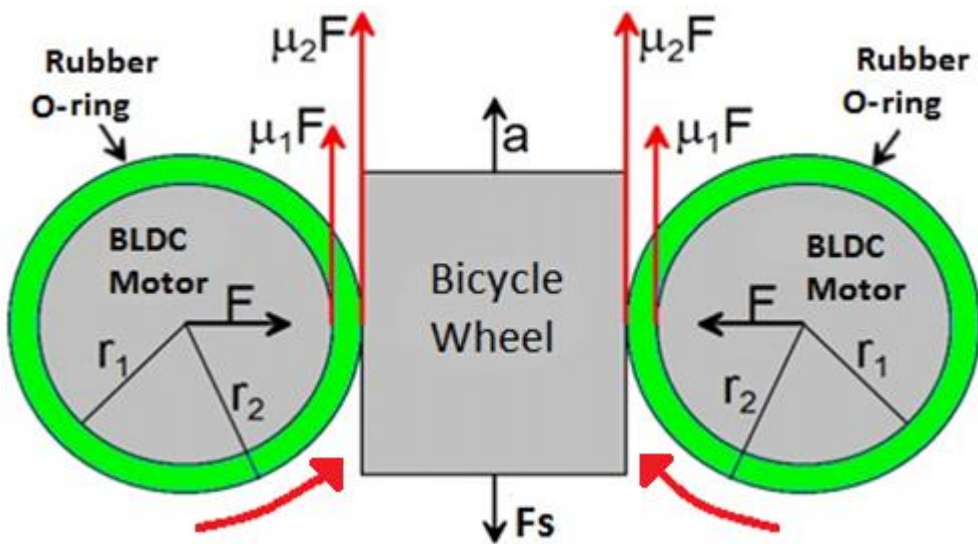


Figure-28 Purposed traction system for BLDC electric bicycles

- F is the force pushing the motors to the wheel.
- F_s is the friction force between bicycle tier and road.
- a is the force produced by the BLDC motors.
- $\mu_1 F$ is the friction force inside of BLDC motor.
- $\mu_2 F$ is the friction force between rubber O-ring and bicycle tier.

Designing the main schematic

After choosing the BLDC motor, it is time to design the BLDC motor controller board. For the motor controller brain, an Arduino Nano (Atmega-328p) was chosen for easy and fast prototyping and to drive the 3-phase inverter. IR-2301 high and low side driver was suitable for this application. To design the Driver board, Proteus CAD platform was used.

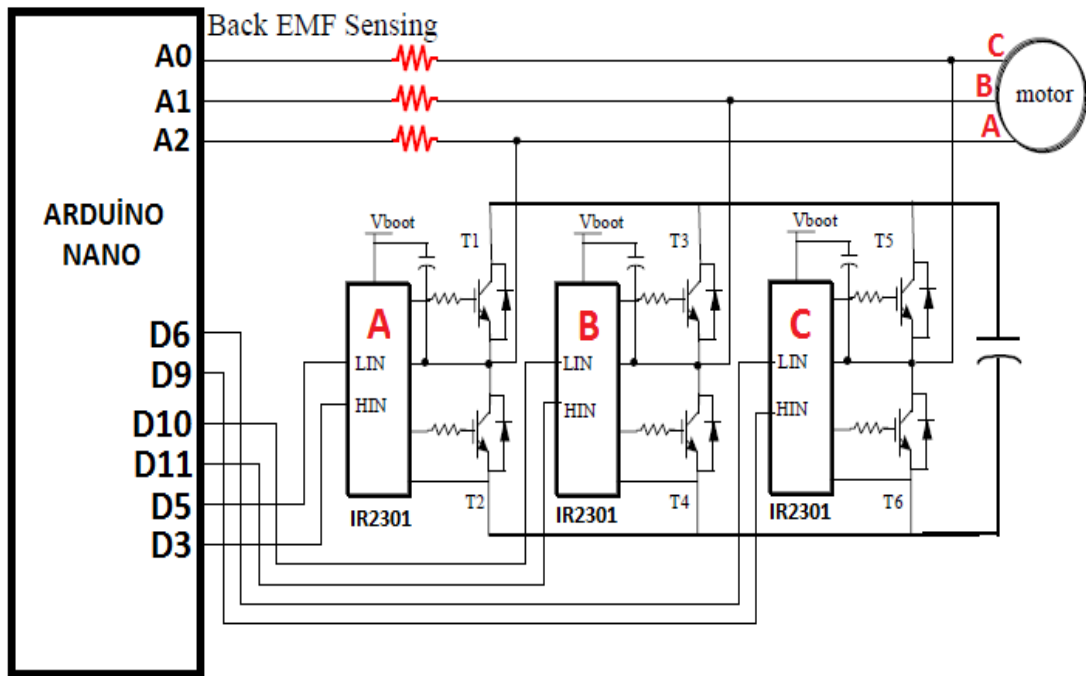


Figure-29 Version (1.0) power electronics schematic

BLDC motor driver board (Version 1.0)

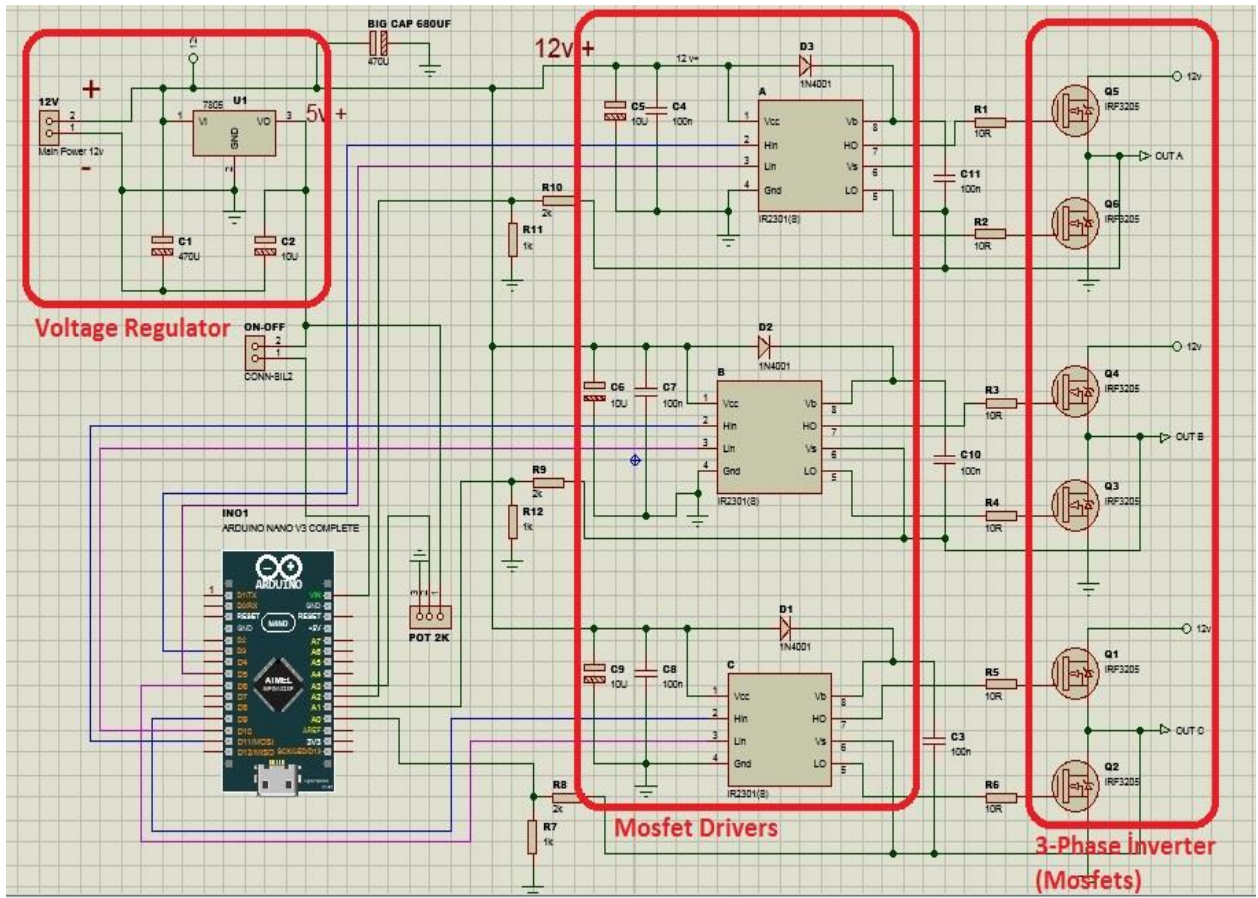


Figure-30 The complete schematic of the motor controller

Voltage regulator

In first version of the board to supply the Arduino, a voltage regulator was used to reduce the power supply voltage for microcontroller working voltage level, which is 5V dc. The regulator was a 7805 linear voltage regulator. It is a very common regulator for low power conception applications. As a disadvantage, it has very low efficiency like (56%). However, since Arduino has a low power consumption like (200mA-300mA) it has enough power for this application.

High and low side drivers

MOSFET drivers were used in this implementation. Due to the Arduino, digital output voltage is 5V and MOSFET's threshold value is approx. (4.5V-5.5V) to activate the MOSFET. It is necessary to apply a voltage higher than threshold value. For commutate precisely the MOSFET using a driver is mandatory.

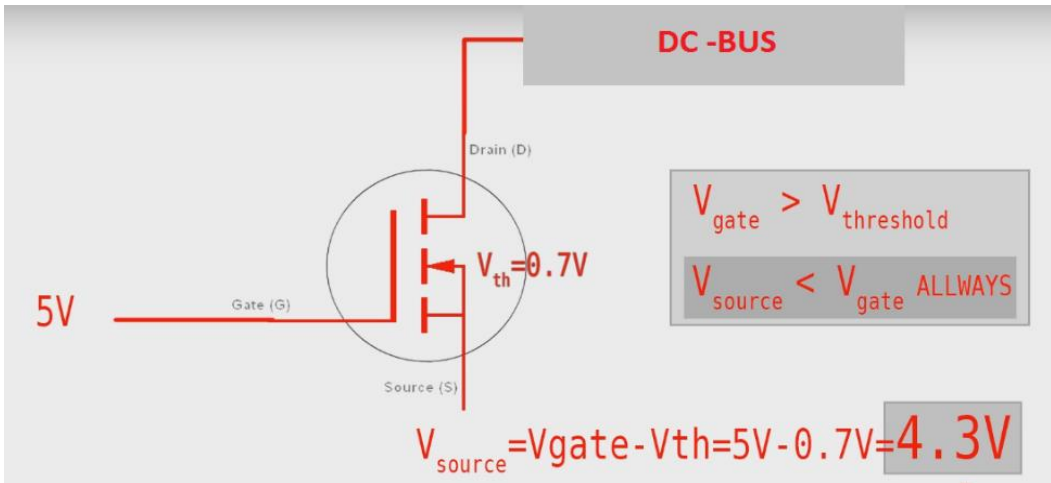


Figure-31 MOSFET schematic explanation (V_{th} = Threshold)

When is applied a 5V dc to gate of the MOSFET, due to the diode inside of the MOSFET the voltage of the $V_{source} = 4.3V$, as illustrated in Figure-31, but we want to drive the BLDC at 12V or higher voltage. In this point, we need the use MOSFET driver to obtain 12V or higher voltage of the source.

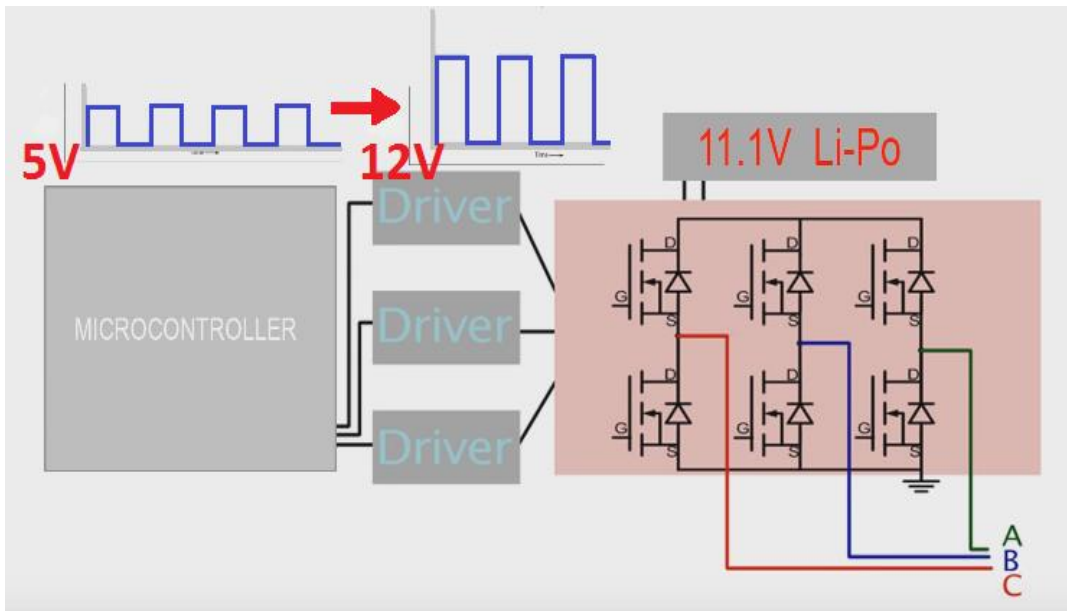


Figure-32 MOSFET driver representation

The MOSFET driver adjusts the voltage from an Arduino pin to properly drive the potential at each phase. Figure-32 is a simplify version of Figure-29. In the Figure-32, we can see the PWM signal voltage amplified to the 12V potential.

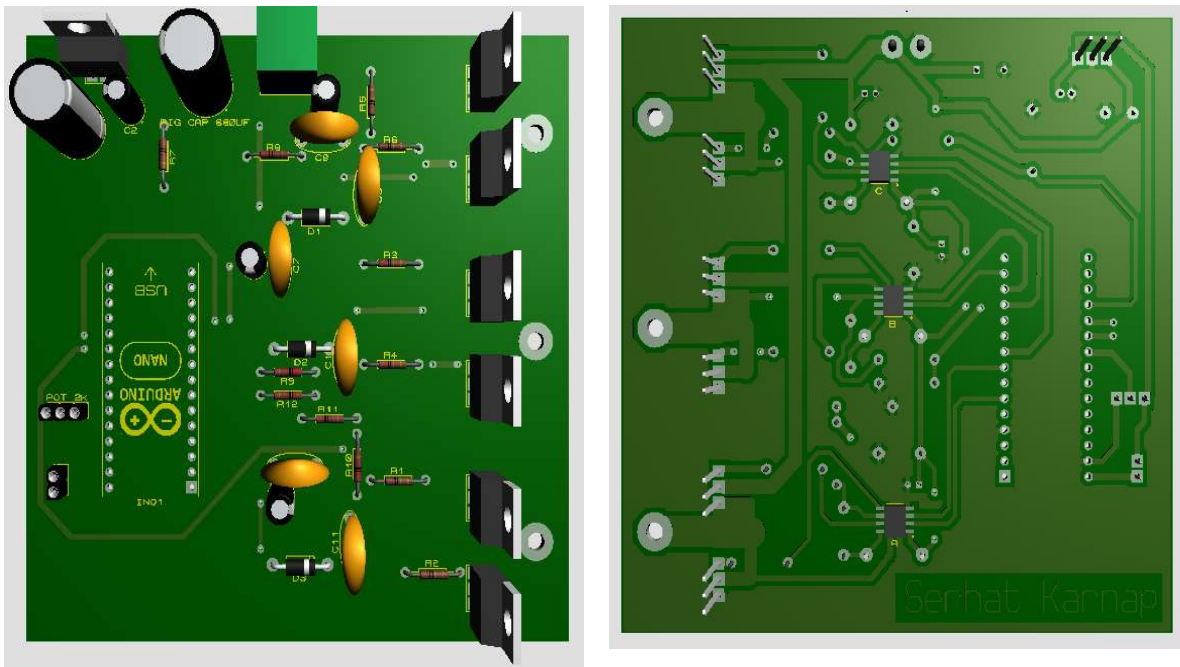
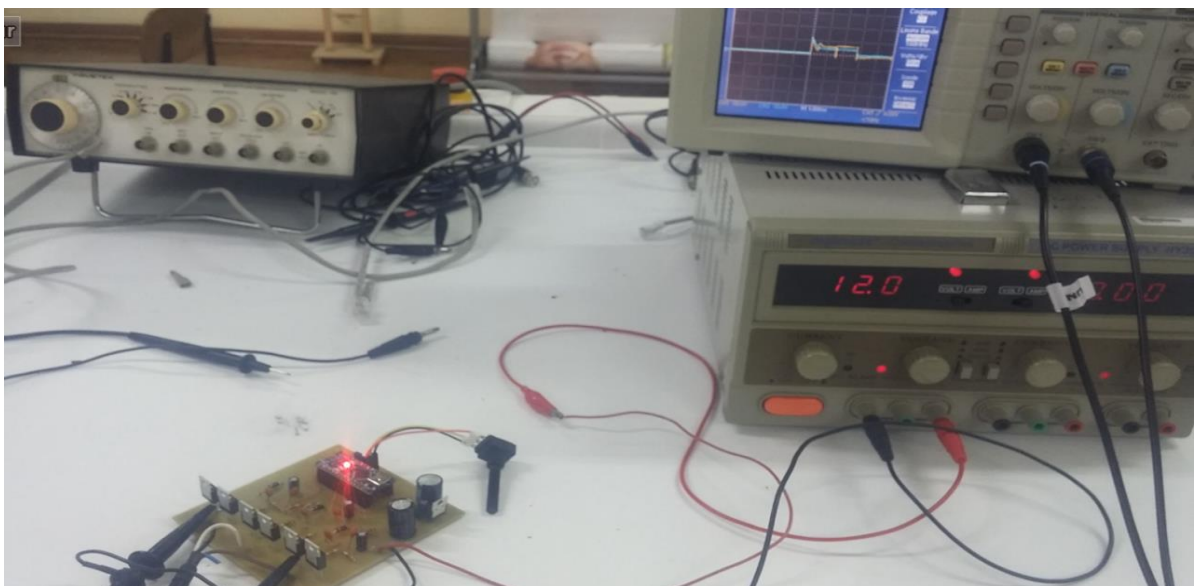


Figure-33 3D model of motor controller

The track going from power to the MOSFETs has to be very thick due to the high current that it delivers. The thickness of the track was calculated by online simulator for 80A current as 1,7mm wide that will be enough for a 34um thickness PCB. To further improve power dissipation over the tracks the traces can be covered with solder, reducing the trace resistance at the same time. This solution presents less power losses on the board and less heat losses on the PCB.

First test and controlling



Figrue-34 First test setup

First, it was tested the board without Arduino and checked the connection and voltage level of each component, plug-in the microcontroller and send the code ready to test. The power supply in the lab can deliver up to max 4A. However, to spin the motor requires more than 8A that is why at the first test the microcontroller get in to loop. To prevent this it was necessary to reduce the current, so some resistors here added to each phase of the BLDC motor. Firstly, 1 ohm resistors each phase were used.



Figure-35 Adding resistors to each phase

Version (1.0) driver board conclusions

The main problem of version (1.0) is the small capacitor value on the 12V main power line. BLDC motor has very low resistance on the coils (~0.8 Ohm) and very high inductance. When we try to drive this type of load, the load acts like a short circuit for dc voltage and these cause high current spikes on the power line. These high current spikes get it into power supply short circuit protection and drops the power line voltage to 0V. When the power line voltage drops to 0V, the microcontroller is resetting itself and this cycle continues.

To prevent this unwanted behavior the input capacitor capacitance has to be increased. Another problem was the voltage regulator since the 7805 has very low efficiency causing overheating problems on its package.

BLDC motor driver board (Version 2.0)

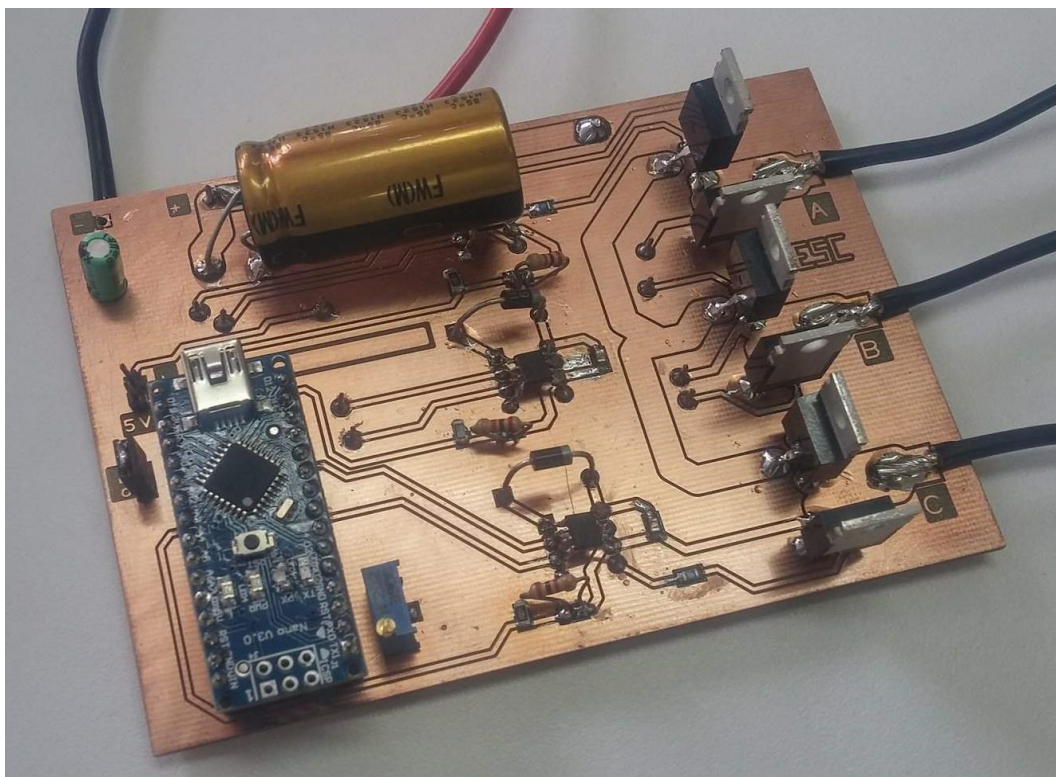


Figure-36 Version 2.0 controller board

The V2.0 in the theory is the same board but with some upgrades.

1. Board is smaller. Version 1.0 is (10cmx10cm) size but version (2.0) is (10cmx8cm) size.
2. The input capacitor capacity has increased from 470uF to 3300uF to reduce the noise and current spikes.
3. The voltage regulator was changed to a more efficient linear regulator, a AMS1117 (5V), which has 70% efficiency, thermal shut down and current limitation features.
4. It was used a two layer PCB, increased the track width to reduce the track resistance and power losses on the board, making it capable of flowing more current to the motor.

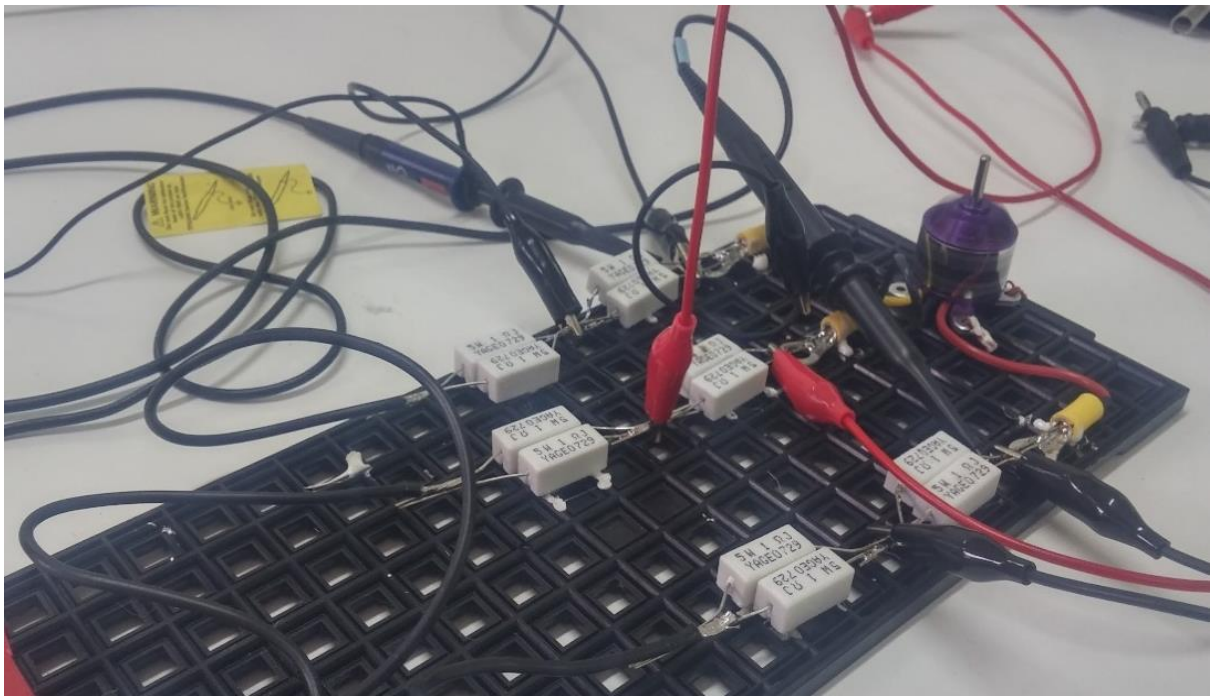


Figure-37 New current limiting resistor configuration

The resistors were connected in parallel to dissipate more power and reduce the back EMF attenuation as showed in Figure-37. The developed board had already voltage divider resistors to reduce the 12V-20V potential to the 0V-5V for microcontroller detection potential capability.

To overcome back EMF attenuation, the configuration of resistors in each phase (illustrated in Figure-37) were changed to two ohm for each phase, enough to limit the current up to 4.5A. Still on the load, there were troubles to drive motor at lower speeds. Therefore, to overcome the problem, the resistors were changed again to only 1-ohm resistor connected to each phase. Moreover, a PC power supply was now used to get enough current.

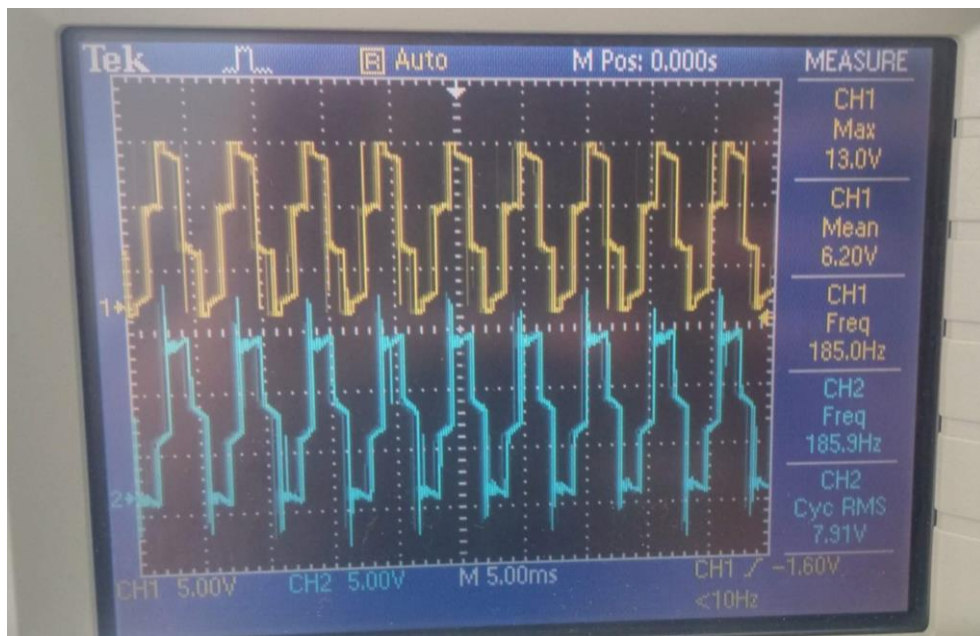


Figure-38 PWM scope outputs of 2 phases maximum throttle

In Figure-38 is shown a first test of version (2.0) at 40 % throttle and a PWM signal frequency of 185 Hz. In addition, the current is about 7.44A.

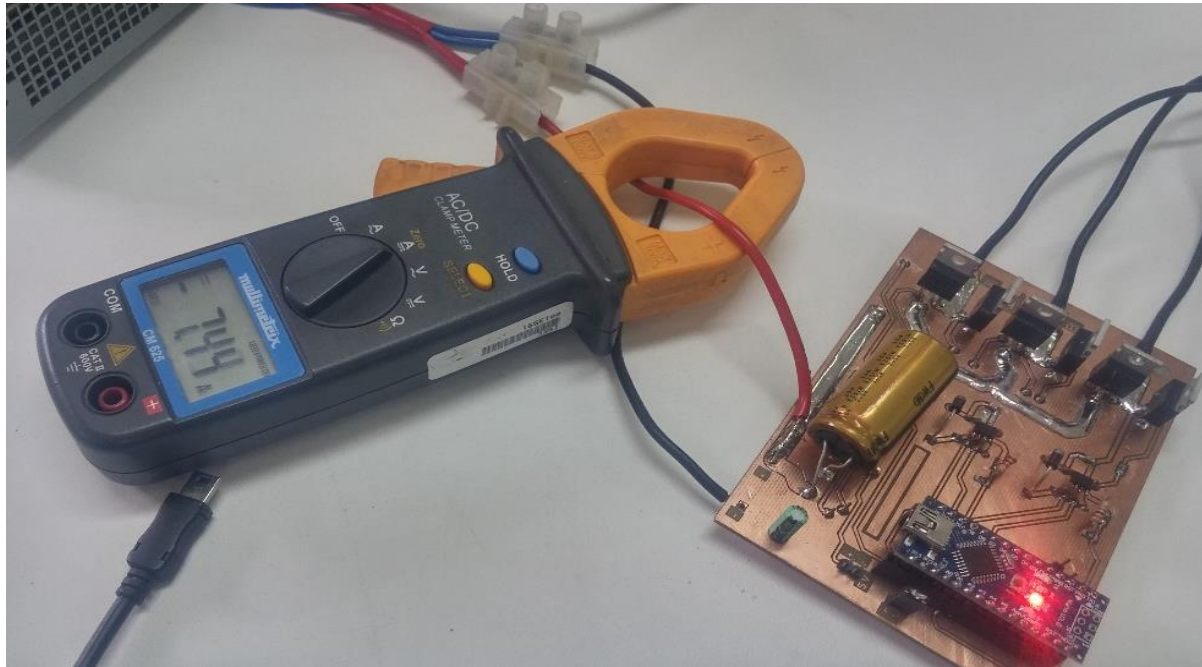


Figure-39 Current measuring from main DC-Bus

Version (2.0) driver board conclusions

The version (2.0) was working without any problems. However, the drive technique of conventional 120° PWM was causing overheating problems on the BLDC motor due to the long duty cycle causing high current spikes on the power line and high harmonics. Summing these problems, we will have an overheating problem. Without any load on the motor, with 7.44A current, after 60sec. the motor temperature was higher than 70°.

In conclusion, the motor driver was working, but the limitation of microcontroller capabilities and limited time, this driving technique was not generating enough power to drive a bicycle and cause overheating problems.

Moreover, when we spin the motor without any power from by BLDC motor controller, the motor is acting as a generator and is inducting current on the stator wirings, as mentioned before on back EMF. If we spin the motor fast enough, this back EMF generate 5V on the Arduino analog input and this will cause the Arduino to turn it on itself without any power connection to power supply!

However, in the future work I would like to use this EMF force as a regenerative breaking on the bicycle and store this energy back to the batteries. To achieve this feature it is necessary to isolate the microcontroller and power electronics. For these reason it was decided to use optic isolators on the new version of controller. With optic isolation, it will be able to drive high voltages without any power problems due to the voltage dropping and auto resetting on the microcontroller. For these reasons the ground terminal has to be separated from power side and microcontroller side.

BLDC motor driver board (Version 3.0)

In this version of board, it was used optic isolator between microcontroller and MOSFET driver. New features of this version:

- Optic isolation
- DC-DC 5V isolation
- Voltage regulator for optic isolators

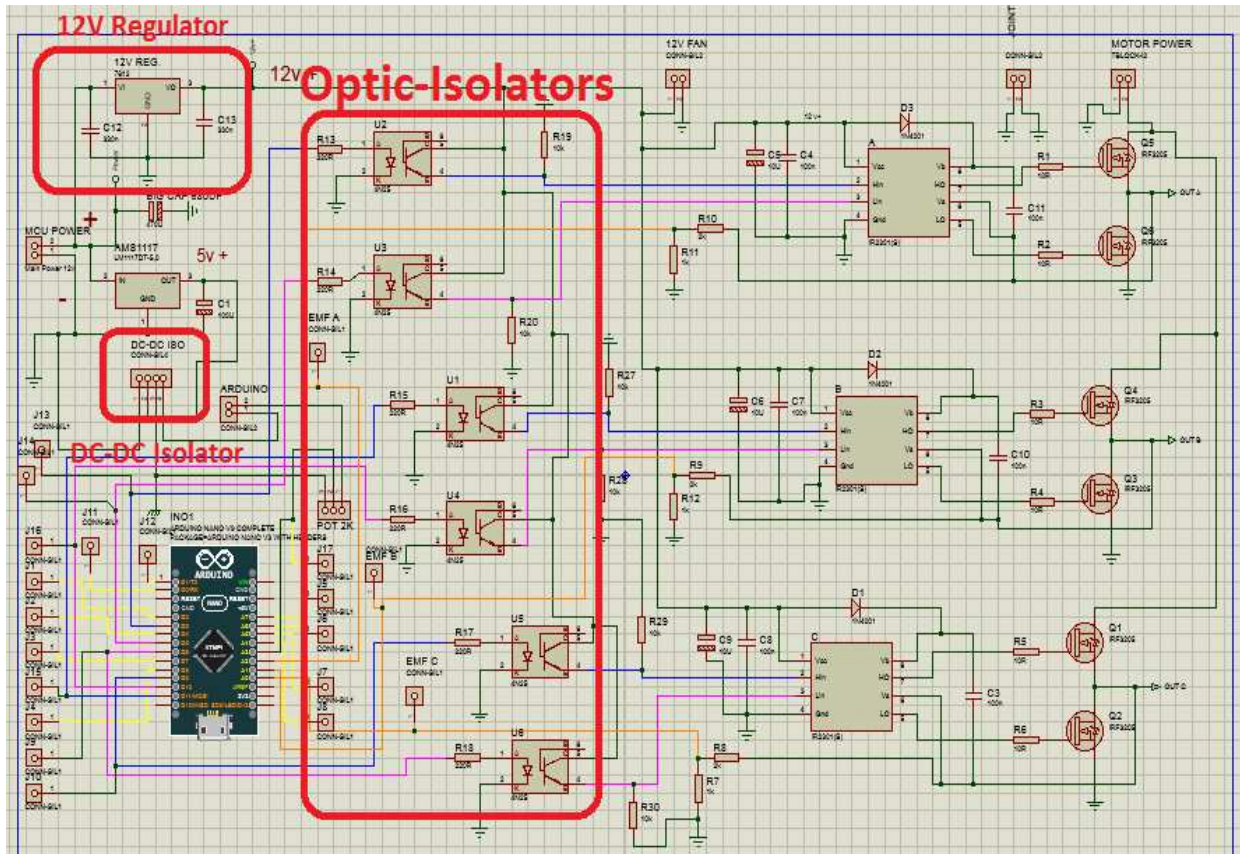


Figure-40 Version (3.0) controller board

The basic design of an opto-coupler, also known as an opto-isolator, consists of a LED that produces infrared light and a semiconductor photosensitive device that is used to detect the emitted infrared beam. Both the LED and photosensitive device are enclosed in a light-tight body or package with metal legs for the electrical connections as shown. An opto-coupler or opto-isolator consists of a light emitter, the LED and a light sensitive receiver, which can be a single photo-diode, phototransistor, photoresist or photo-SCR, or a photo-TRIAC with the basic operation of an opto-coupler.

Assume a phototransistor device as shown in Figure-41. Current from the source signal passes through the input LED that emits an infrared light whose intensity is proportional to the electrical signal. This proportional signal gives an analog output on the emitter.

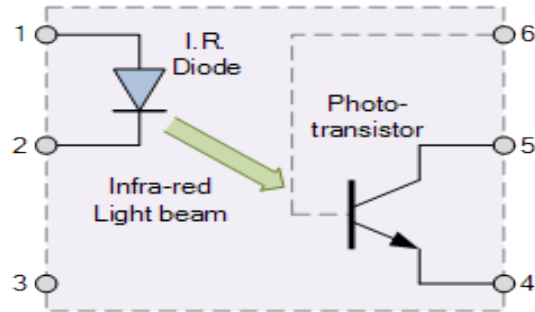


Figure-41 Opto-coupler schematic

This emitted light falls upon the base of the phototransistor, causing it to switch ON and conduct in a similar way to a normal bipolar transistor. The base connection of the photo-transistor can be left open (unconnected) for maximum sensitivity to the LEDs infra-red light energy or connected to ground via a suitable external high value resistor to control the switching sensitivity making it more stable and resistant to false triggering by external electrical noise or voltage transients [54].

The phototransistor can be used to switch current in the output circuit. Since there is no direct electrical connection between the input and output of an opto-coupler, electrical isolation up to 10kV is achieved.

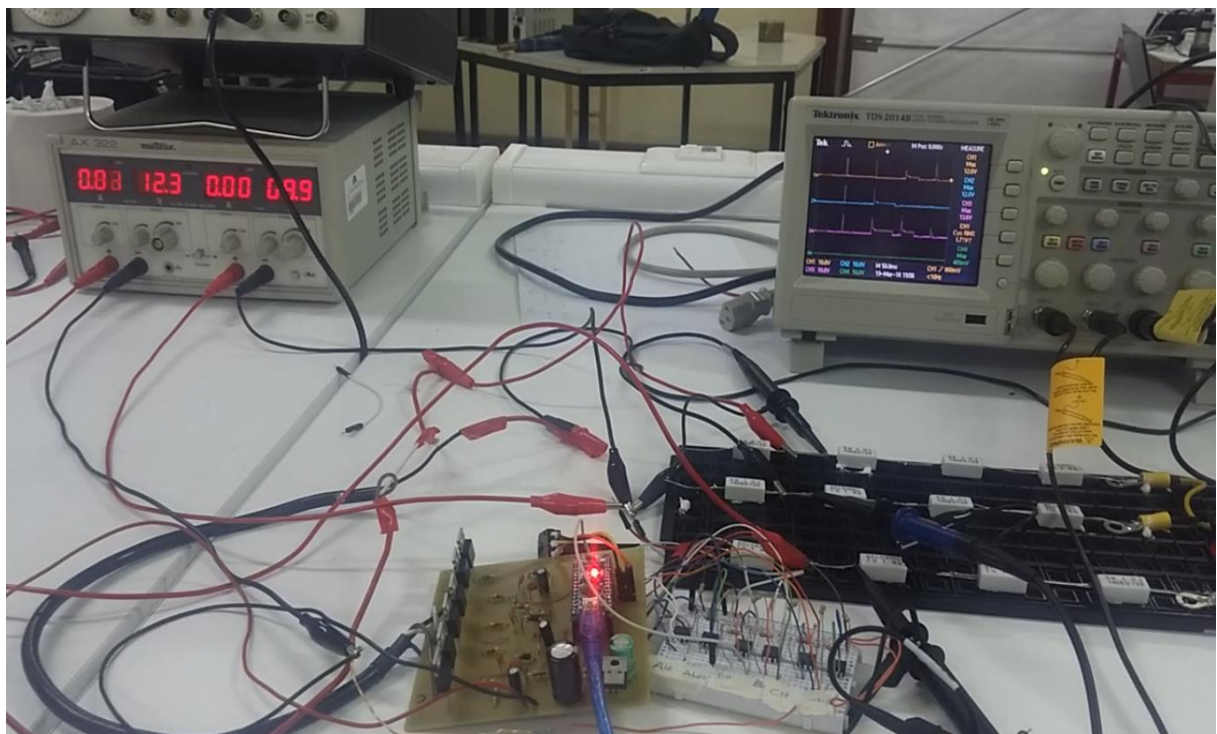


Figure-42 First test of the Optic Isolators

Common applications for opto-couplers include microprocessor input/output switching, DC and AC power control, PC communications, signal isolation and power supply regulation, which suffer from current ground loops, etc.

In this test circuit, opto-couplers are used to isolate the signal passing to the motor driver. In case of any voltage spikes or short circuit, opto-couplers will protect the microcontroller. In addition, high current or high voltage applications the electromagnetic interference can cause a problem to low power electrical control signals.

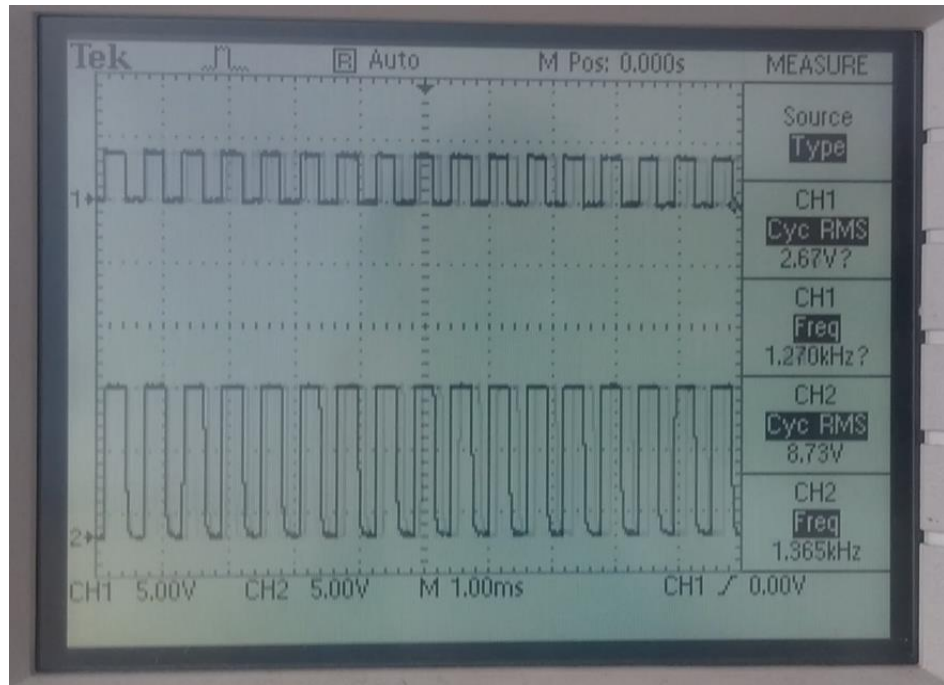


Figure-43 Opto-coupler frequency testing

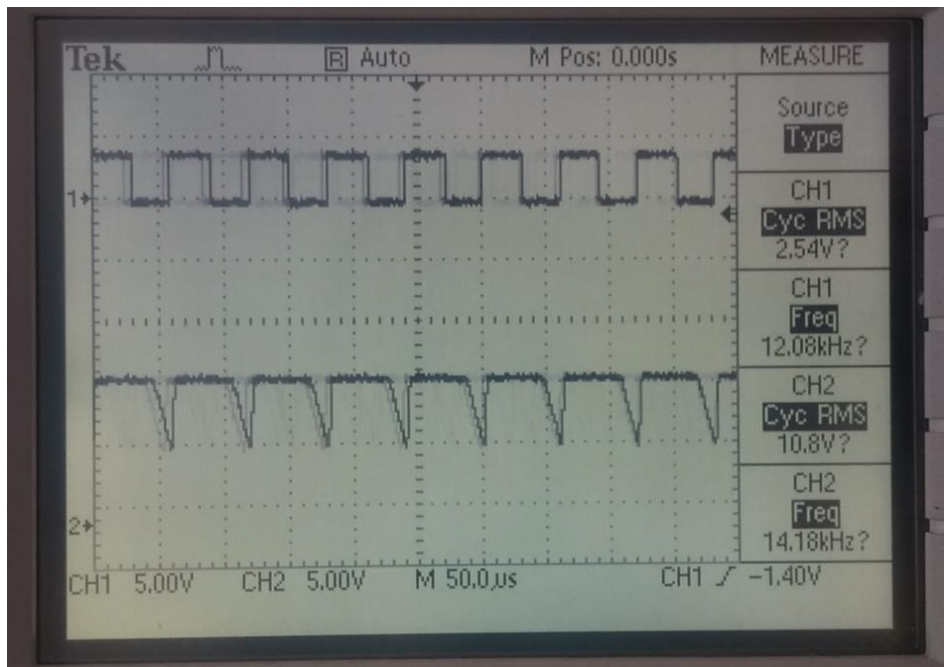


Figure-44 Max Opto-coupler frequency before get in the saturation

In Figure-43, we can see the square signal on the opto-coupler input and output while testing with signal generator. It was also tested to make sure that the saturation frequency seen in Figure-44 is higher than the motor driver frequency. Otherwise at the higher speed we will lose the shape of the square wave commutation signal, which can cause wrong commutation, to drive motor at higher speeds. However, as our driving frequency is max. 1~3 kHz, this will not cause any problems for this controller.

DC-DC Isolator

Power supply designers often use isolated DC/DC converters to realize galvanic isolation, meet safety requirements and enhance noise immunity. When designing an isolated DC/DC converter, output voltage regulation accuracy is one of many design objectives to consider and the required level can vary from one application to another. Better than $\pm 5\%$ overall voltage regulation is necessary in some cases while $\pm 10\%$ might be adequate for others.

Like a transformer, it can be used to step-down or step-up a DC voltage source. DC converters can also be used as switching mode regulators to convert a DC voltage, normally unregulated, to a regulated DC output voltage.

Using a DC-DC isolated converter, the power to supply the microcontroller becomes independent from sudden (short time voltage drops) current spike effects on the motor side.

After adding the opto-couplers and dc-dc isolators, it was needed to supply these chips that are working at 12V, so our main input voltage could be 12V-24V in respect to the max v_{cc} value of the MOSFET driver, and opto-coupler. Then it was used a 12V linear voltage regulator to supply the MOSFET driver, opto-coupler and external air-cooling fan to dissipate the heat on the MOSFETs.

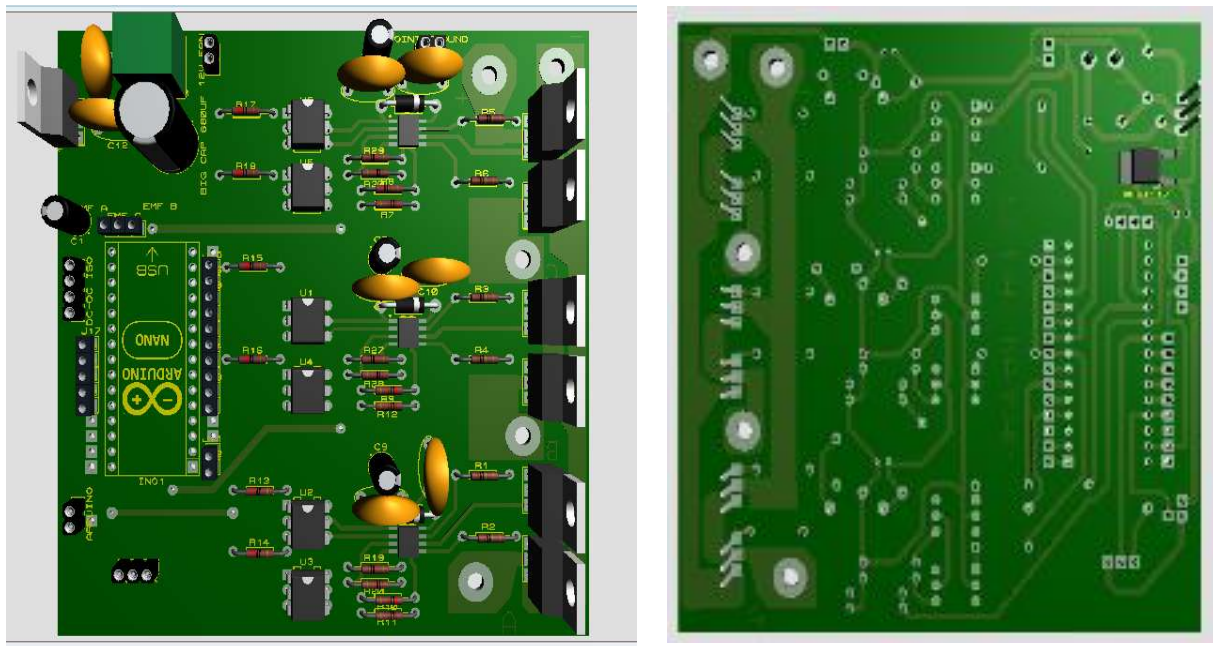


Figure-45 3D schematic BLDC driver board V3.0

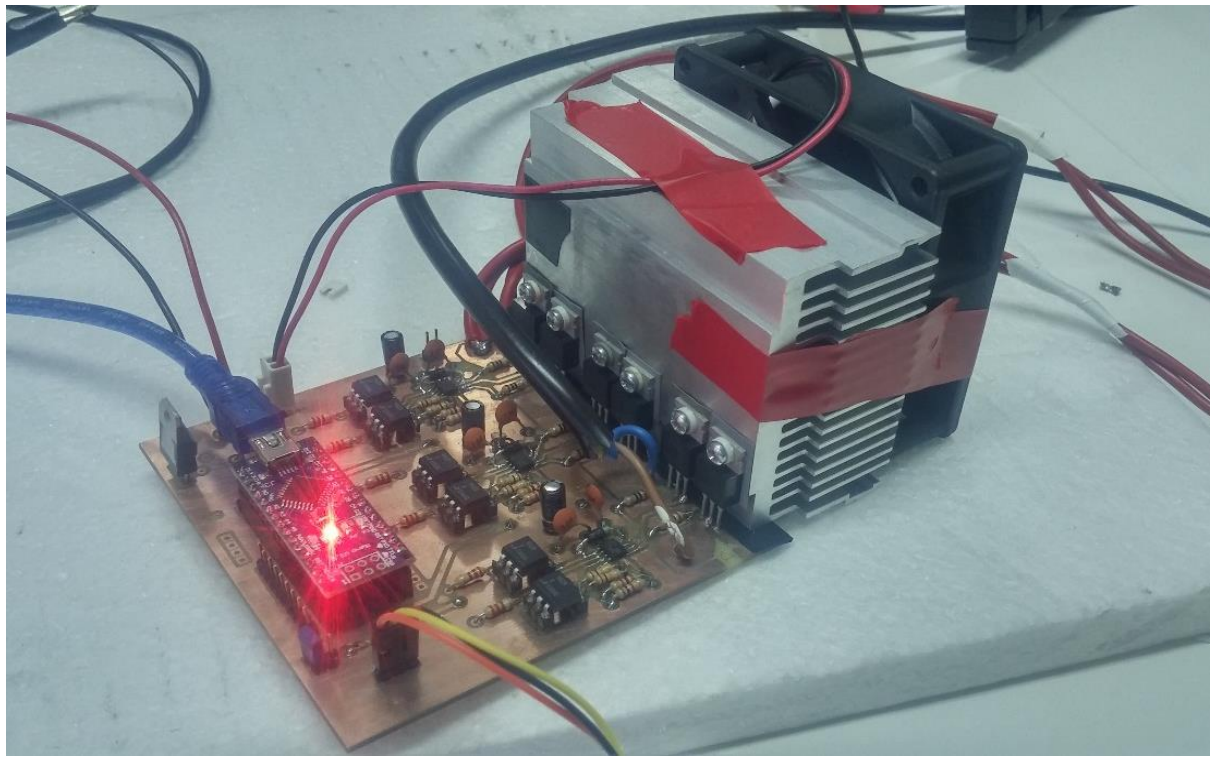


Figure-46 Version (3.0) BLDC motor controller

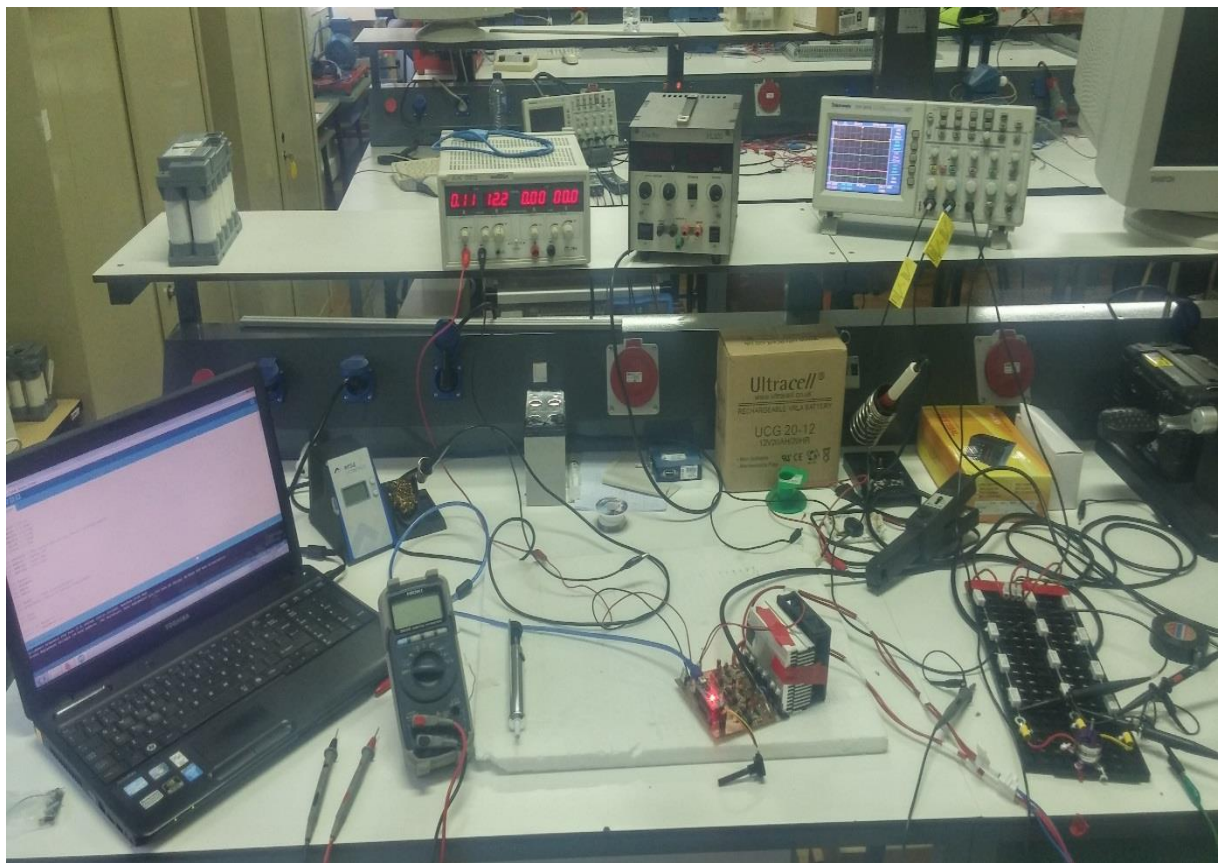


Figure-47 Test setup of Version (3.0)

The BLDC back EMF detection software

First, it is measured the voltage drop on each three inputs. Moreover, the sum of these three values is made. This sum will be our zero point.

```
void loop() {  
  
    int emA = analogRead(emfA);  
    int emB = analogRead(emfB);  
    int emC = analogRead(emfC);  
    int sum = (emA+emB+emC)/3;  
  
    unsigned long currentMillis = micros();  
  
    if(currentMillis - previousMillis >= Delay) {  
        previousMillis += Delay;  
    }  
}
```

Figure-48 Zero crossing point calculations

Time is measured using micro function to control the sequence speed that is needed to execute Motor step sequence loop. The step delay value is controlled by a potentiometer (as described in Figure-51 code).

```
//Phase1 C-B  
switch(fase){  
    case 1:  
        digitalWrite(AA1,LOW);  
        digitalWrite(AA2,LOW);  
        digitalWrite(BB1,LOW);  
        digitalWrite(CC2,LOW);  
        digitalWrite(BB2,HIGH);  
        digitalWrite(CC1,HIGH);  
        delta = emA-sum;  
  
        break;  
  
    //Phase2 A-B  
    case 2:  
        digitalWrite(AA2,LOW);  
        digitalWrite(BB1,LOW);  
        digitalWrite(CC1,LOW);  
        digitalWrite(CC2,LOW);  
        digitalWrite(AA1,HIGH);  
        digitalWrite(BB2,HIGH);  
        delta = emC-sum;  
        break;  
}
```

Figure-49 Cases of MOSFETs controlling sequence

This loop is our switch case functions. In each case microcontroller, set to high just two pins for two MOSFET's of the triple phase bridge. The rest of the pins are set to low. This delta variable is very important. We know that we have a zero crossing measured voltage from

negative to positive values or from negative to positive, and use the actual delta and last delta to control that for example.

If the last delta was negative and the actual delta is positive, it is clear that we have a zero crossing from negative to positive values. If the deltas are vice-versa, we will have a cross from positive to negative. (Figure-50).

We will have six cases when we reach the sixth one we go back to the first one. This is the sequence loop.

```

if (Lastdelta < 0) {
    if (delta > 0)
    {
        Lastdelta=delta; //save the last delta
        fase= fase + 1;
        if (fase > 6) {
            fase = 1;
        }
    }
}
//Zero cross from - to +
if (Lastdelta > 0){
    if (delta < 0)
    {
        Lastdelta=delta;
        fase= fase + 1;
        if (fase > 6) {
            fase = 1;
        }
    }
}
//Zero cross from + to -

```

Figure-50 Comparing the zero crossing

Using software to detect the zero crossing back EMF has the advantage of eliminating the noise. In the virtual neutral point technique, back EMF detection is a big problem, as even using a low pass filter cannot compensate the all the effects of the noise. In this case we must measure the SNR (Signal to Noise Ratio) is high enough for the detection of BLDC motor angular position.

```

int t =analogRead(IN); //From the potentiometer
Delay=map(t,0,1024,1,1000); //we obtain the delay speed using the potentiometer
//we map the values from 1 to 1000 microseaconds

```

Figure-51 The reading of the potentiometer value

Conclusion of back EMF BLDC sensorless motor drive

Without any sensor feedback from BLDC motor, with the help of the back EMF detection technique, detecting the motor position is possible. However due to the time, budget and equipment limitation, the design hardware implemented for the BLDC motor drives of the gates of the MOSFETs is the conventional 120° PWM. This produces overheating problems on the motors because it does not use any current chopping technique.

Moreover, the motors available for this project did not have enough power to drive a bicycle continuously. To overcome this problem another controller board was made using hall sensors to track motor positioning. In the next chapter, we will take a closer look on how to design a sensored BLDC motor driver controller.

Furthermore, performed experiments made with commercial ESC's Figure-52 also confirms the commercial ESC's using a current chopping technique to drive a BLDC motor without overheating problems.

1. Current Chopping Technique

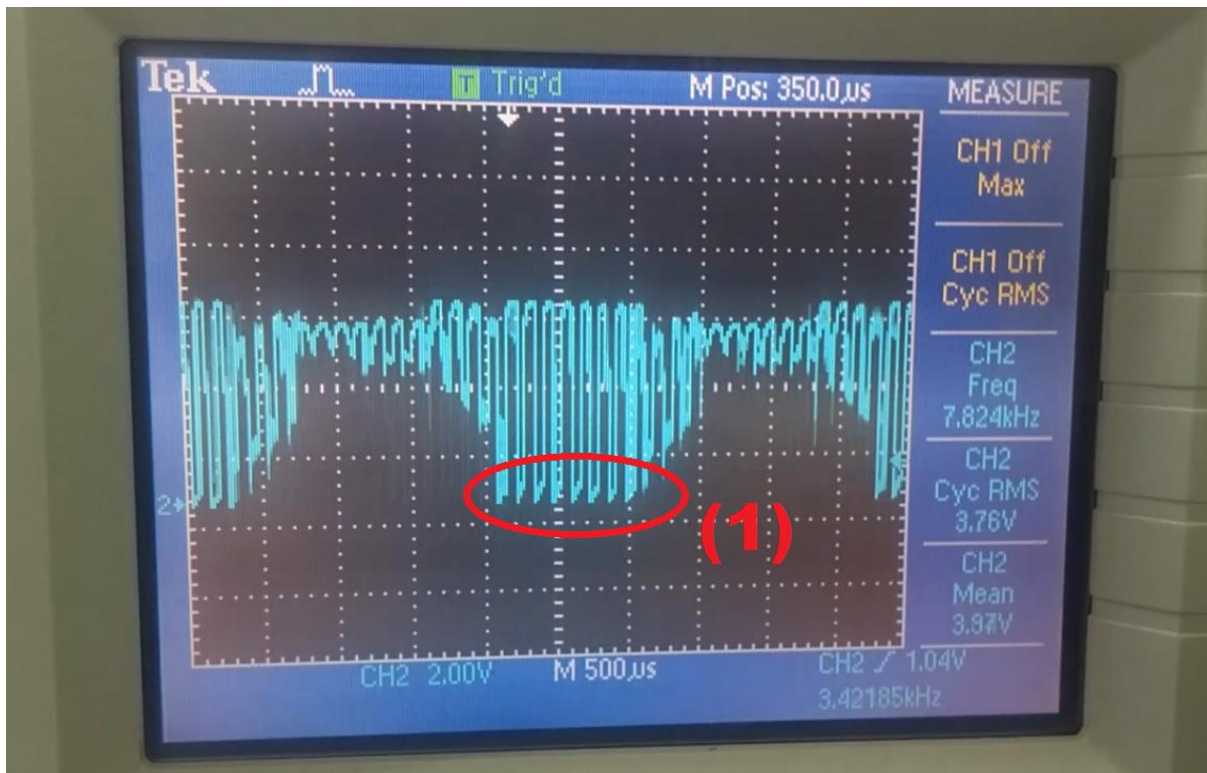


Figure-52 Commercial ESC phase scope output 50% throttle

CHAPTER 6

Development of a Sensored BLDC motor drive

The Hall Effect encoder system consists of three sensors, which detect the magnetic field of a magnet, which passes across the sensors. The three sensors are equally spaced to cover one electrical rotation. In other motor types, which do not use permanent magnets in the rotor, the sensor is placed on the output shaft. The shaft then has a number of magnets on it matching the pole-pair parameters of the motor. With BLDC motors, it is possible to utilize the existing permanent magnets in the rotor for Hall Effect sensing. Hall sensors on stator are shown in Figure-54. The hub motor available in the lab had damaged Hall sensors, so they were replaced by new ones, and to achieve that, the hub motor was opened from both sides as shown in Figure-53.



Figure-53 Sensor replacement to the motor stator

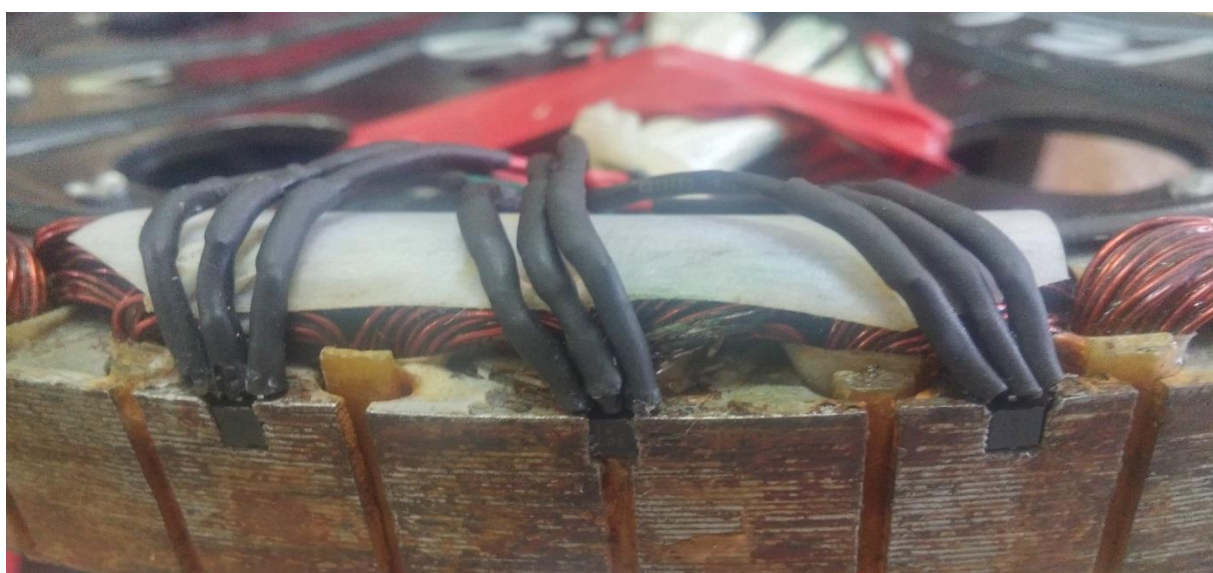


Figure-54 Hall sensors replacement from motor stator

Each Hall Effect sensor outputs a high signal for one magnetic pole, and a low signal for the other magnetic pole. As the rotor advances through one electrical rotation, both the north and south magnetic poles pass across each sensor. The result is a half-duty square wave output. The three sensors are spaced 120° apart.

From the figure below, it is quite clear that they produce six evenly spaced high/low transitions from the three sensor outputs. Each of these transitions indicates that a commutation step transition should occur.

The controller software developed for this sensored motor type has a lookup table, which tells it which commutation step should occur related to each Hall Effect encoder state. This table varies by controller, depending on the alignment of the sensors with the rotor and the motor winding connections.

A typical configuration is to have hall sensor one aligned with the BEMF across the M2-M1 connections, hall sensor 2 aligned with M3-M2, and hall sensor 3 aligned with M1- M3, where M1, M2, and M3 are the output terminals of the controller connected to the phase windings. The Hall Effect outputs should be a square wave representation of the BEMF. An example table is given below corresponding to the Figure-55.

Step	Hall A	Hall B	Hall C	Code	A (M1)	B (M2)	C (M3)
1	1	0	1	101	+Vm	-Vm	Float
2	1	0	0	100	Float	-Vm	+Vm
3	1	1	0	110	-Vm	Float	+Vm
4	0	1	0	010	-Vm	+Vm	Float
5	0	1	1	011	Float	+Vm	-Vm
6	0	0	1	001	+Vm	Float	-Vm

Figure-55 Commutation sequence according to the Hall sensors outputs [55]

According to the working principle, a new schematic was designed, which can also drive CD-ROM motors as an optional, with available amplified input pins for CD-ROM motors.

Version 1.0 BLDC sensored motor driver

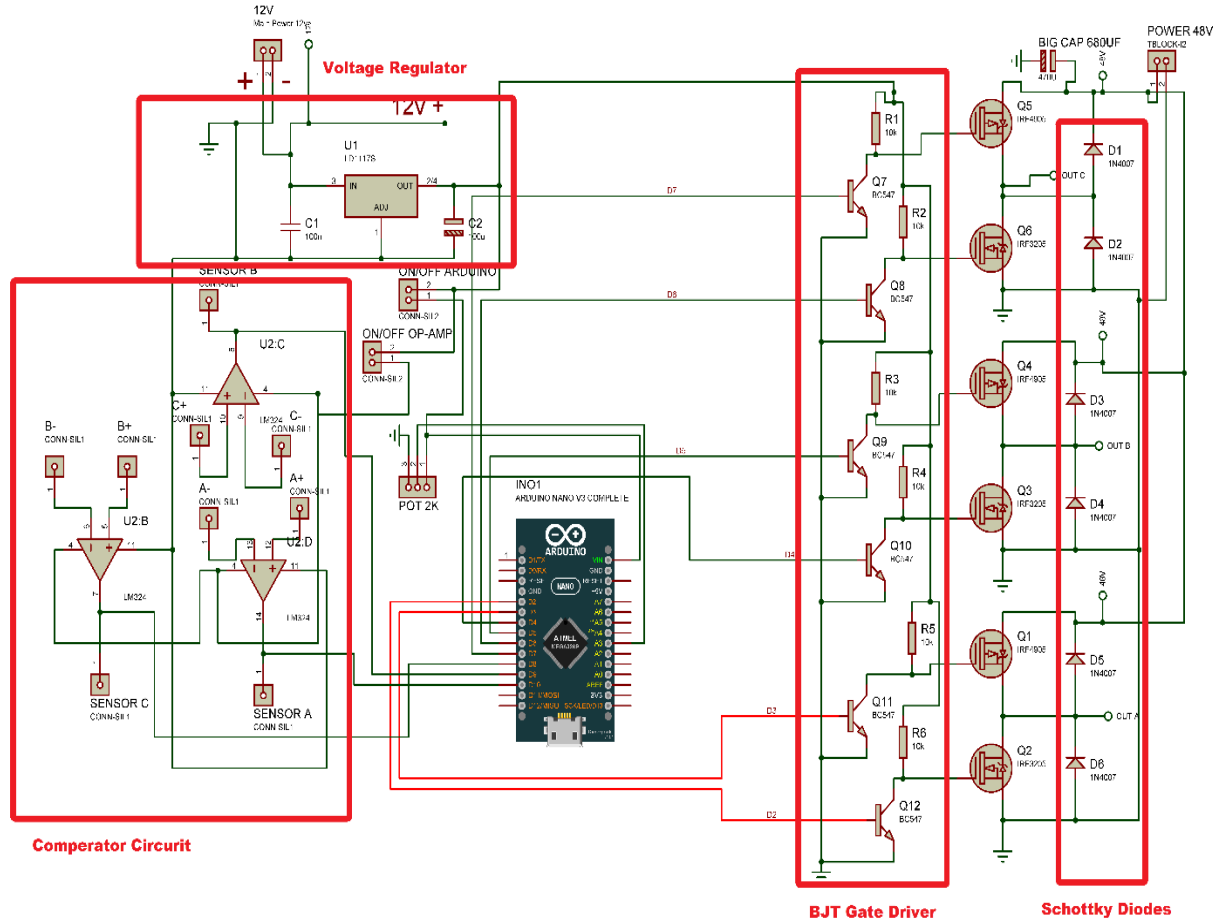


Figure-56 Sensored BLDC motor driver schematic version (1.0)

This time it was decided to experiment to use BJT transistors as a gate driver of the MOSFETs to keep the schematic simple. Moreover, it was also decided to use schottky diodes. As schottky diodes are much faster than normal diodes inside of the MOSFETs they can eliminate much faster EMF oscillations that come from the BLDC motor phases, which will increase the life time of MOSFET's.

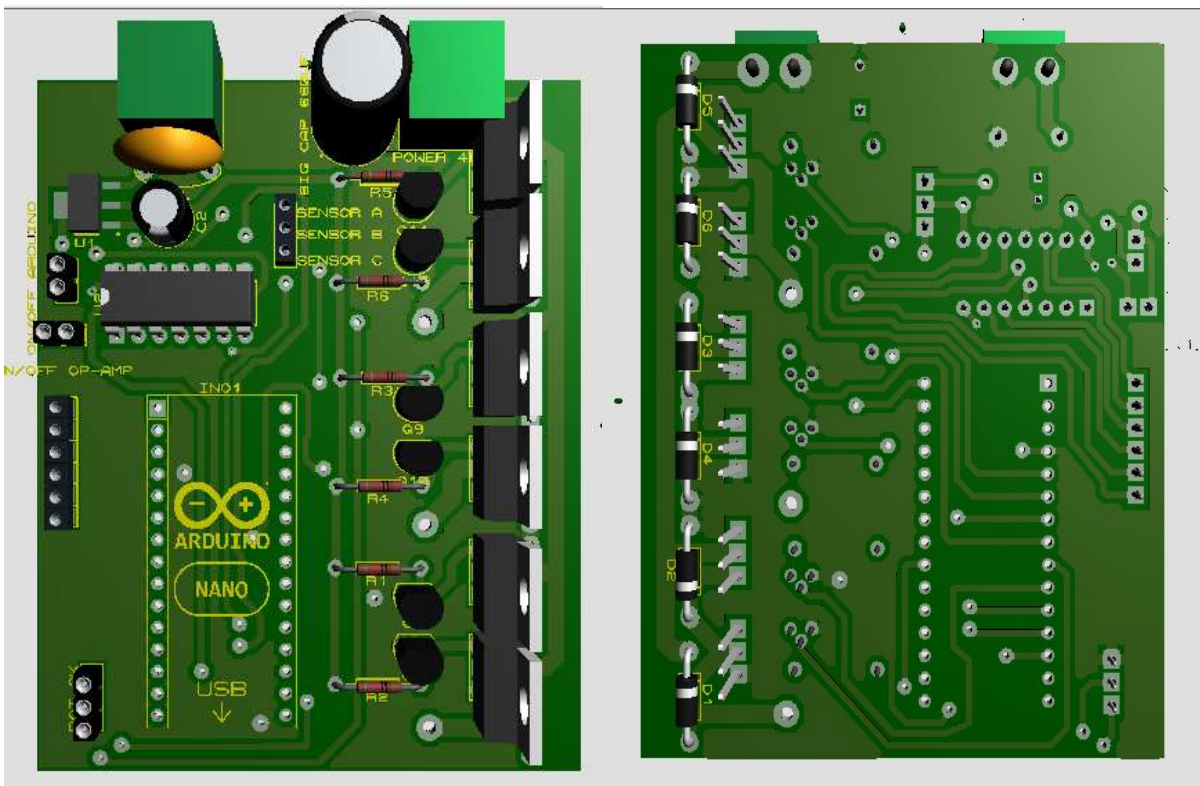


Figure-57 3D View of Version (1.0)

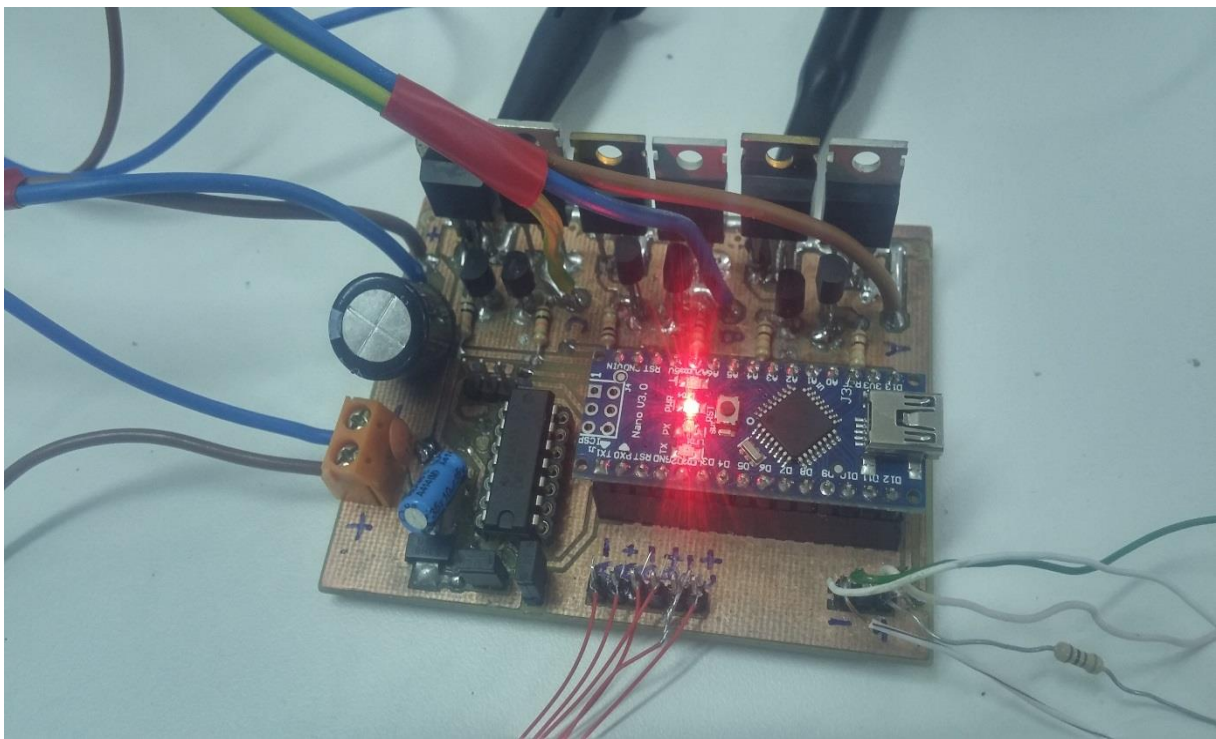


Figure-58 First setup for Version (1.0)

Version (2.0) BLDC sensored motor driver

For the new version of BLDC motor driver, to keep the things simple, it was used a schmitt trigger IC to drive the P-Channel MOSFET's being easier writing software. Moreover, it was used also a MOSFET driver IC to Drive the MOSFET's more efficient.

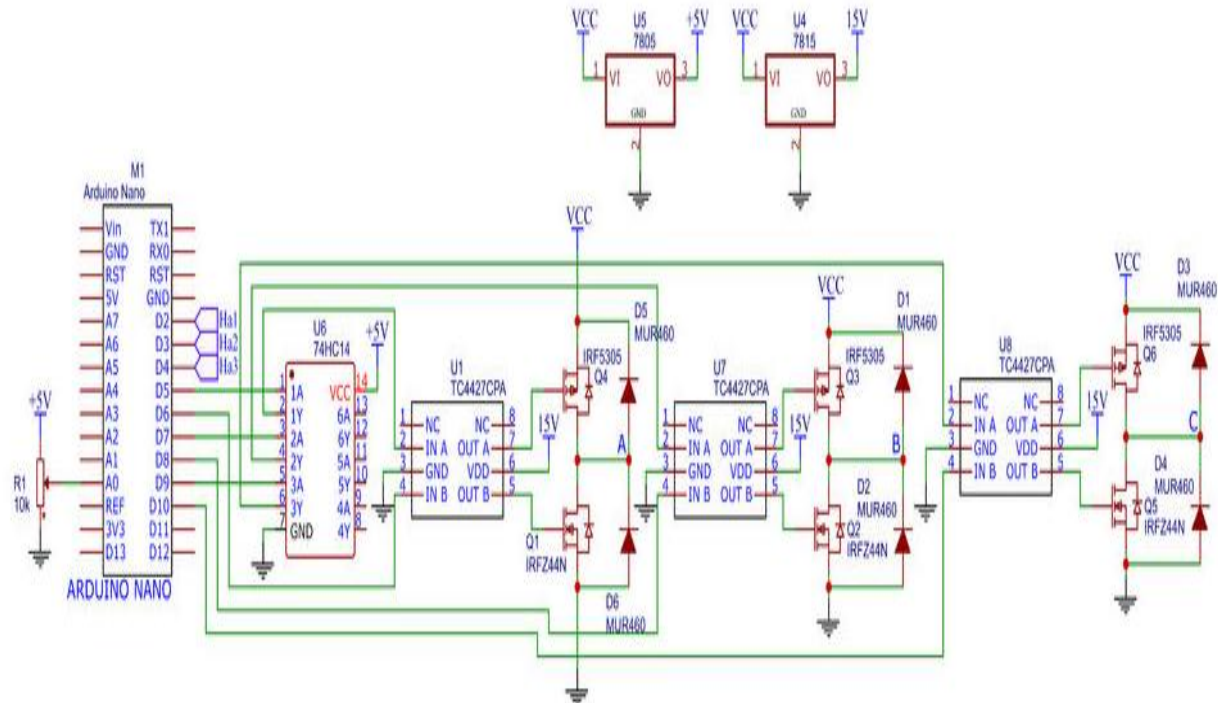


Figure-60 Schematic of BLDC sensored motor driver version (2.0)

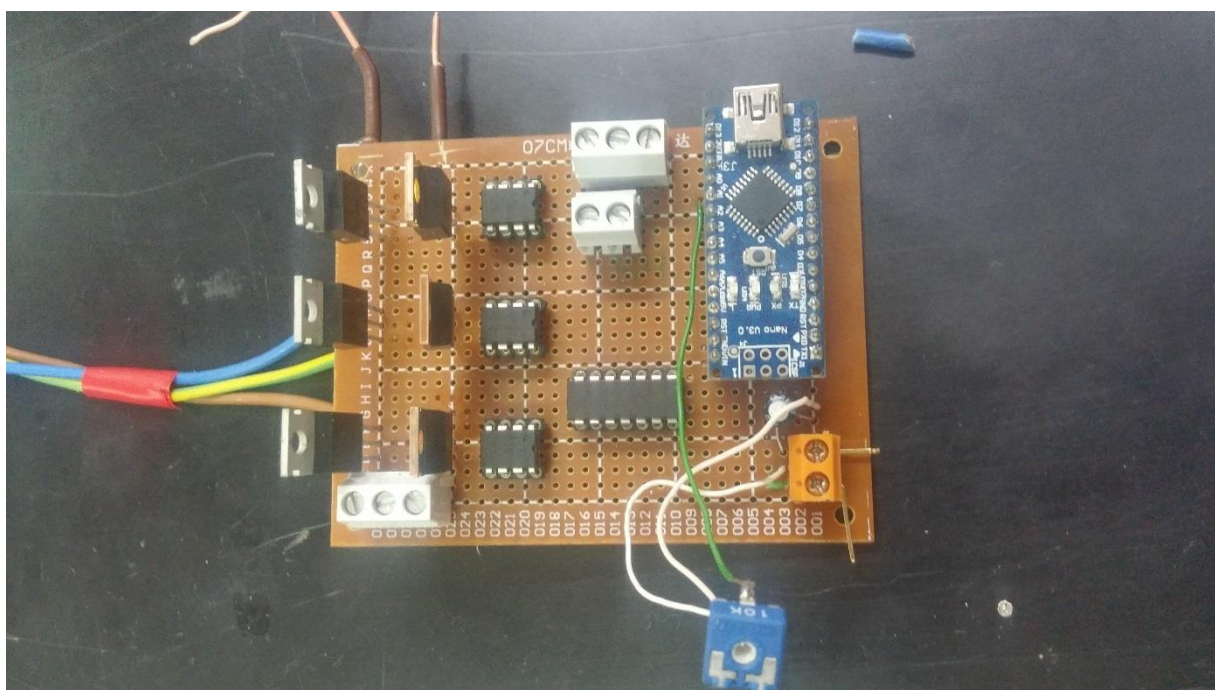


Figure-61 Due to time limitations this new version was made on a prototyping board

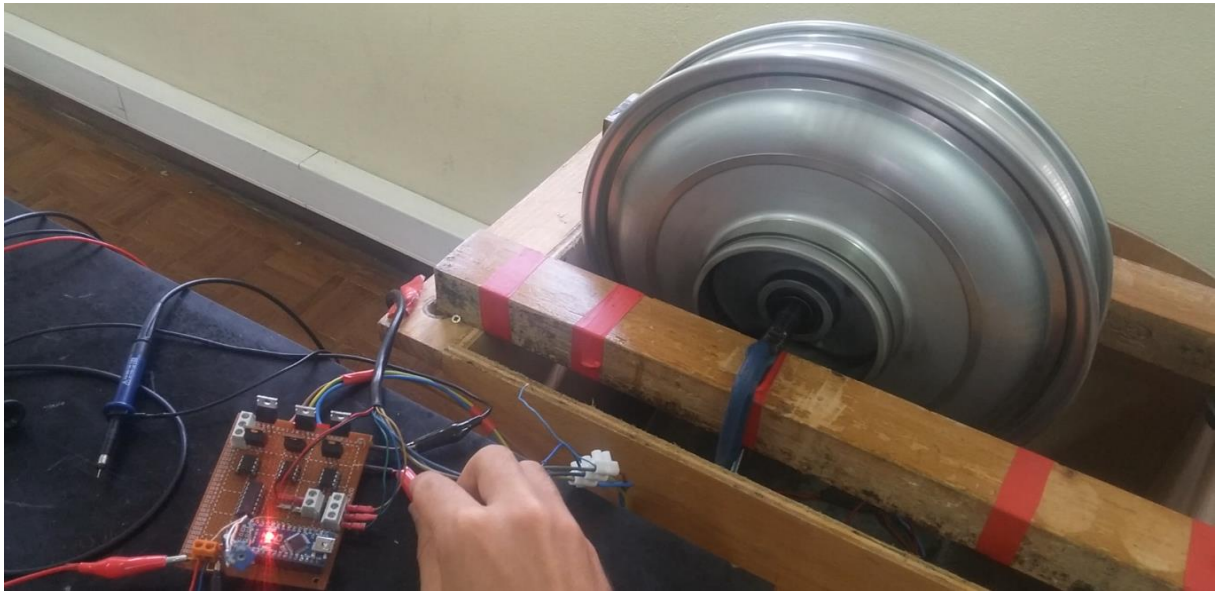


Figure-62 First test setup of sensored motor driver V2.0

The main contactor circuit

The main contactor board see in Figure-63 consist of four relays to switch the power connection safely. The four automotive relays 12V-40Amps allow to disconnect or connect the motor from the motor driver. To drive the circuit it was used one push button to control the relays. When the push the button is activated, the relays are closed and connection between motor and motor driver is established. To observe the status of the relays, a RGB LED strip was used. When the relays are closed and motor driver connected to the motor LED strip lights up green, meaning that ignition is on and the bicycle is ready to go. If we push again the button will open and LED strip lights up red which means that motor driver and motor are disconnected.

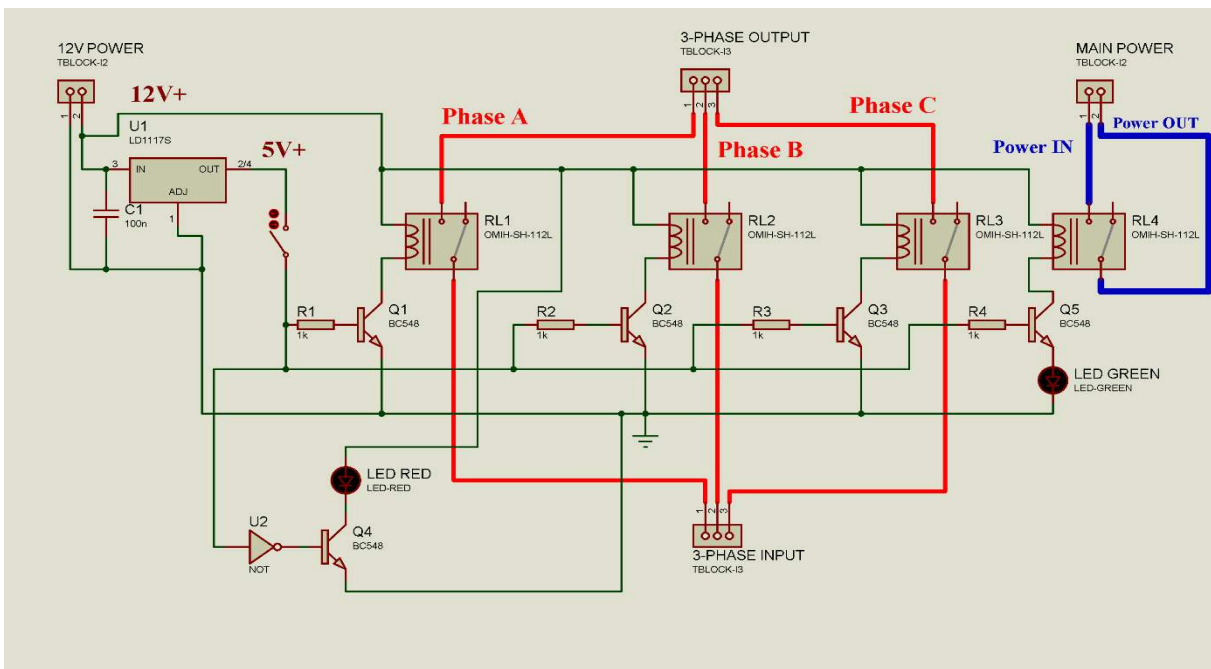


Figure-63 The complete contactor circuit

This contactor circuit allows to disconnect the motor from driver in case of emergency. This circuit can also be improved by adding a current sensing sensor to give information to cut the motor power in case of over current situations.

Moreover, this circuit can also be used for regenerative breaking features. To achieve the regenerative breaking, we must disconnect the motor driver from motor to direct all current coming from motor to rectifier circuit. We can separate the motor from the motor driver. Changing the software to while making regenerative breaking the commutation must be stopped.

Final test and assembly

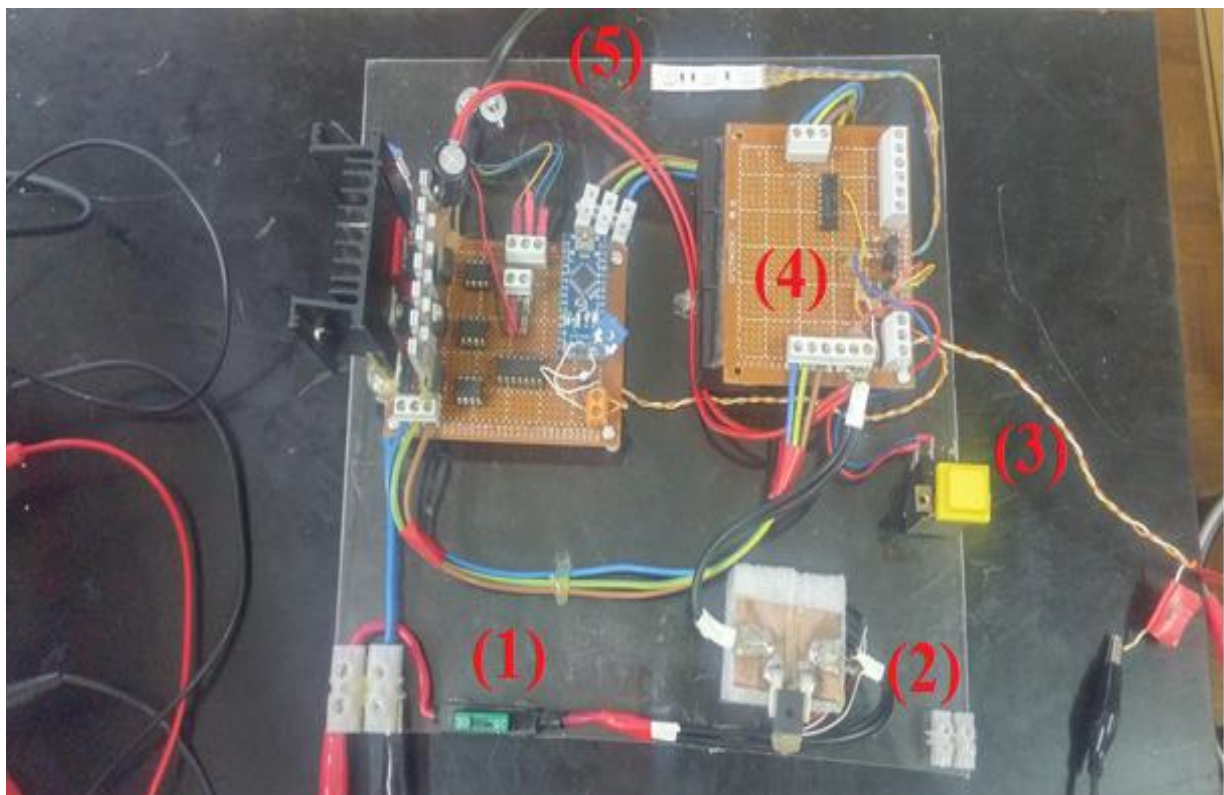


Figure-64 The final design

As shown in Figure-64 the final design has the following parts:

1. The safety fuse 30Amps
2. The Hall Effect current sensor
3. Ignition On/Off switch
4. The main contactor circuit
5. Ignition status LED

Due to the time and budget limitations a Hall Effect current sensor was not connected to another microcontroller to achieve overcurrent safety features. Overcurrent safety features allow us to sense the DC-Bus current and at the desired value, if the current reaches the desired value to disconnect the motor by sending a logic signal to main contactor board.

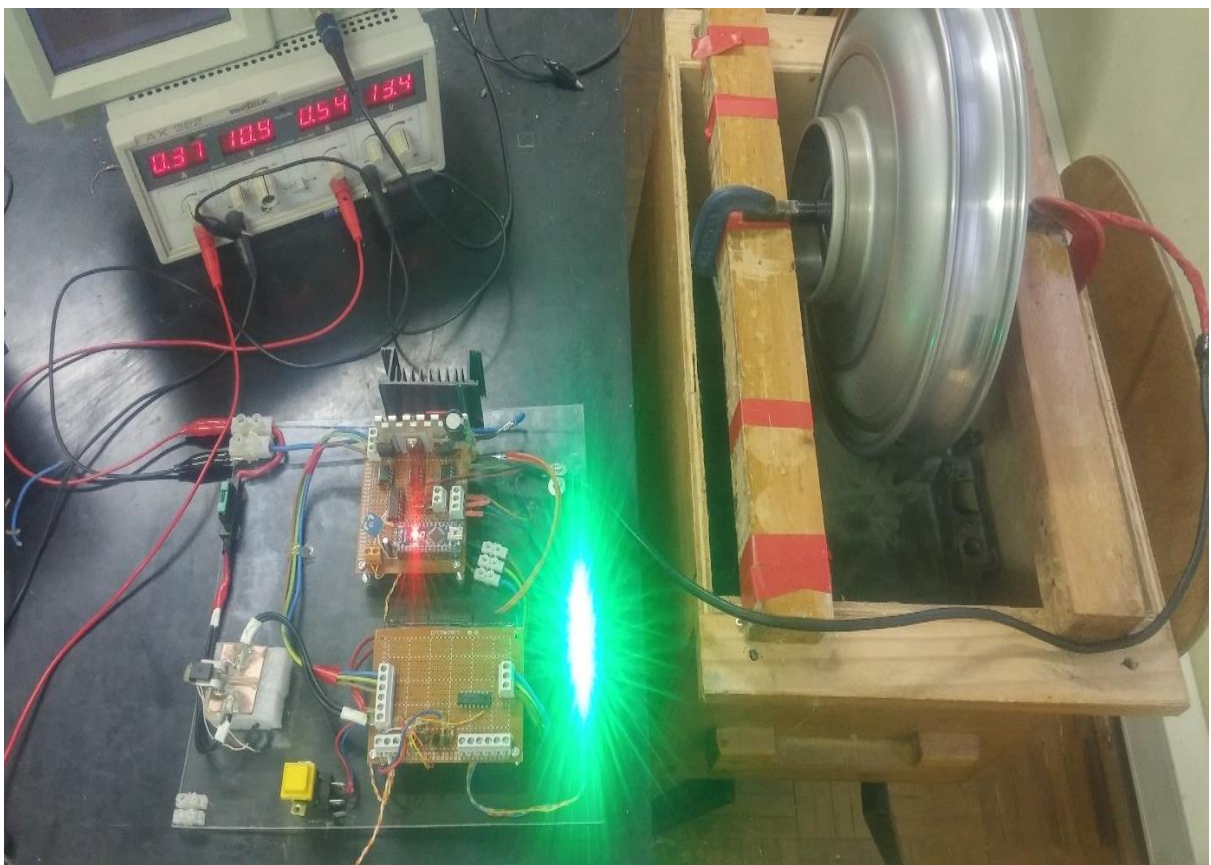


Figure-65 The final system of sensored motor

CHAPTER 7

Conclusions and Future Work

Using basic 8-bit microprocessor like the Atmega328p, it is possible to drive sensored BLDC motors without problems. Since the Hall Effect, sensors giving the motor position as a logic output to the 8-bit microprocessor is capable to drive the motor up to 10 kHz frequency.

Moreover creating virtual neutral point for BLDC, motor and applying filtering it is possible to detect exact position of the motor. However, this time the commutation is the problem as in this sensorless driver board we are not using the current chopping technique to reduce and prevent high current flowing to the coils. Due to high current rises, overheating is causing problems on the motor. To implement the current chopping technique without measuring the current flowing at each phase of the motor was not possible due to the slow response of Atmega328p ADC. Moreover, measuring high current requires more advanced current sensing techniques and complex microcontrollers like (32-bit or 64-bit Arm Processors) should be used.

However, using basic microcontroller helps a lot to understand design, implementation and understanding working principle of BLDC motor drivers. In this report due to the time and budget, limitations it was not implemented the purposed electric bicycle traction method to the bicycle.

The future work should be use more powerful sensored BLDC motors and to implement purposed traction method using 3D printed parts to the bicycle. Also, using more advance microcontrollers like the STM32 and special 3-phase motor driver IC's to measuring the current to each phase will allow to use current chopping technique to prevent the motor from overheating.

Furthermore, using the relay system we designed in Figure-68 disconnecting to the motor from driver and with the 3 phase rectifying circuit we can use BLDC motors as a generator and convert the kinetics energy of bicycle to electrical energy. This systems allows regenerative breaking and energy storage back in to batteries, which also increases the range of the electric bicycle.

To summarize the conclusions for this report, understanding the control technique for BLDC motor and designing a BLDC motor controller board to a traction system in real world applications was achieved, learning also some of the related difficulties.

REFERENCES

1. Lenihan, J. (2008). *Bilim İş Başında*, Tübitak Yayınları September 2008, Ankara.
2. Tuncay, R. N., Ustun, O., Yilmaz, M., Gokce, C., ve Karakaya, U. (2011). Design and implementation of an electric drive system for in-wheel motor electric vehicle applications, Vehicle Power and Propulsion Conference, Chicago, IL, 1-6, 6-9 September.
3. <https://www.slideshare.net/amol.vidwans/tpdroid-electric-cycle-kit> Date: 24.06.2018 - El-Refaie.
4. Starschich, E., and Muetze, A. (2007). Comparison of the performances of different geared brushless-dc motor drives for electric bicycles, IEEE International Conference on Electric Machines & Drives, 1, 140 – 147.
5. Adams, W. (1884). Electric motor, *United States Patent*, No: 300827, Date: 24.06.1884.
6. Morchin, W. C., and Oman, H. (2006). Electric Bicycles-A Guide to Design and Use, Mass: IEEE Press Series on Electronics Technology.
7. Wilson, D. G., Papadopoulos, J., and Whitt, F. R. (2004). Bicycling Science, Cambridge, MIT Press.
8. Adams, W. (1884). Electric motor, *United States Patent*, No: 300827, Date: 24.06.1884.
9. Steffens, M. J. (1898). Bicycle, *United States Patent*, No: 613732, Date: 08.11.1898.
10. Libbey, H. W. (1897). Electric bicycle, United States Patent, No: 596272, Date: 28.12.1897.
11. Morchin, W. C., and Oman, H. (2006). Electric Bicycles-A Guide to Design and Use, Mass: IEEE Press Series on Electronics Technology.
12. Wilson, D. G., Papadopoulos, J., and Whitt, F. R. (2004). Bicycling Science, Cambridge, MIT Press.
13. Lin, J., Schofield, N., and Emadi, A. (2013). External-rotor 6–10 switched reluctance motor for an electric bicycle, Industrial Electronics Society, IECON 2013 - 39th Annual Conference of the IEEE, Vienna, 2839 – 2844, 10-13 Nov.
14. Chlebosz, W., Ombach G., and Junak, J., (2010). Comparison of Permanent Magnet Brushless Motor with Outer and Inner Rotor Used in E-Bike, Electrical Machines (ICEM), 2010 XIX International Conference on, 1 – 5, 6-8 September.
15. Lomonova, E. A., Vandenput, A. J. A., Rubacek, J., Herriron, B., and Roovers, G. (2002). Development of an Improved Electrically Assisted Bicycle, Proceedings of 2002 IEEE Industry Applications Society Annual Meeting, 384-389, November.
16. http://www.ebikes.ca/tools/simulator.html?bopen=false&motor=M3007&batt=B4812_MH&cont=C20&hp=150&autothrot=true&throt=76.4&autothrot_b=true&motor_b=M3007&batt_b=B4812_MH&hp_b=150&throt_b=76 Available June 2017.

17. Hendershot J. R., and Miller, T. J. E. (1994). Design of Brushless Permanent Magnet Motors, Magna Physics Publishing and Oxford University Press, USA.
18. Kenjo, T., ve Nagamori, S. (1985). Permanent-Magnet and Brushless DC Motors, Clarendon Press, Oxford.
19. Lai, Y.S.; Shyu, F.S.; Chang, Y.H. Novel Pulse-Width Modulation Technique with Loss Reduction for Small Power Brushless DC Motor Drives. In Proceedings of the Industry Applications Conference (37th IAS Annual Meeting), Pittsburgh, PA, USA, October 2002; pp. 2057-2064; Volume 3.
20. El-Refaie, A. M. (2005). High-speed operation of permanent magnet machines, (PHD Thesis), University of Wisconsin, Madison.
21. Meier, F. (2008). Permanent-magnet synchronous machines with non-overlapping concentrated windings for low-speed direct-drive applications, (P.H.D), Royal Institute of Technology, Stockholm.
22. K.Uzuka, H.Uzuhashi, et al., "Microcomputer Control for Sensorless Brushless Motor," IEEE Trans. Industry Application, vol.IA-21, May-June, 1985.
23. Adnan, A., and Ishak, D. (2009). Finite Element Modeling and Analysis of External Rotor Brushless DC Motor for Electric Bicycle, Research and Development (SCOReD), 2009 IEEE Student Conference on, 376 – 379, 16-18 June.
24. K.Rajashekara, A.Kawamura, et al, "Sensorless Control of AC Motor Drivers," IEEE press, 1996.
25. J.Filla, "ECMs Move into HVAC," Appliance Manufacture, Mar.2002, pp25-27.
26. J.Jancsurak, "Motoring into DSPs," Appliance Manufacture, Sept.2000, pp57-60.
27. Tuncay, R. N., Ustun, O., Yilmaz, M., Gokce, C., ve Karakaya, U. (2011). Design and implementation of an electric drive system for in-wheel motor electric vehicle applications, Vehicle Power and Propulsion Conference, Chicago, IL, 1-6, 6-9 September.
28. D.Peter and J.Hath, "ICs Provide Control for Sensorless DC Motors," EDN magazine, pp.85-94, April 1993.
29. Datasheet of IR2301 from IOR Semiconductor.
30. Microsemi Corp, "Speed Control of Brushless DC Motors-Block Commutation With Hall Sensors", Microsemi Corporation, 2012.
31. <https://www.digikey.ca/en/articles/techzone/2017/jan/why-and-how-to-sinusoidally-control-three-phase-brushless-dc-motors> Available: June, 2016.

32. T.J.E. Miller, "Brushless Permanent-Magnet and Reluctant Motor Drives," Oxford, 1989.
33. R.Becerra, T.Jahns, and M.Ehsani, "Four Quadrant Sensorless Brushless ECM Drive," IEEE Applied Power Electronics Conference and Exposition 1991, pp.202-209.
34. J.Moreira, "Indirect Sensing for Rotor Flux Position of Permanent Magnet AC Motors Operating in a Wide Speed Range," IEEE Industry Application Society Annual Meeting 1994, pp401-407.
35. <https://www.pandaebikes.com/what-is-a-hall-sensor/> Available: Sep 2017.
36. Shao, J.; Nolan, D.; Hopkins, T. Improved Direct Back EMF Detection for Sensorless Brushless DC (BLDC) Motor Drives. In Proceedings of the Industry Applications Conference Eighteenth Annual IEEE Applied Power Electronics Conference and Exposition (APEC 2003), Miami, FL, USA, February 2003; pp. 300-305; Volume 1.
37. Vinatha, U.; Pola, S.; Vittal, K.P. Recent Developments in Control Schemes of BLDC Motors. In Proceedings of the IEEE International Conference on Industrial Technology (ICIT 2006), Mumbai, India, December 2006; pp. 477-482.
38. Position and Speed Control of Brushless DC Motors Using Sensorless Techniques and Application Trends, José Carlos Gamazo-Real *, Ernesto Vázquez-Sánchez and Jaime Gómez-Gil ,Department of Signal Theory, Communications and Telematic Engineering, University of Valladolid (UVA), 47011 Valladolid, Spain.
39. Peixoto, Z.M.A.; Freitas Sa, F.M.; Seixas, P.F.; Menezes, B.R.; Cortizo, P.C.; Lacerda, W.S. Application of Sliding Mode Observer for Induced E.M.F., Position and Speed Estimation of Permanent Magnet Motors. In Proceedings of the 1995 International Conference on Power Electronics and Drive Systems (PEDS 95), Singapore, February 1995; pp. 599-604; Volume 2.
40. <https://www.linearmotiontips.com/what-is-a-chopper-drive-for-a-stepper-motor/> Available: March 2018.
41. L6234 Datasheet BRUSHLESS DC MOTOR CONTROLLER –ST electronics – Page-14.
42. Shao, J.; Nolan, D.; Hopkins, T. Improved Direct Back EMF Detection for Sensorless Brushless DC (BLDC) Motor Drives. In Proceedings of the Industry Applications Conference Eighteenth Annual IEEE Applied Power Electronics Conference and Exposition (APEC 2003), Miami, FL, USA, February 2003; pp. 300-305; Volume 1.
43. Markadeh, G.R.A.; Mousavi, S.I.; Daryabeigi, E. Position Sensorless Direct Torque Control of BLDC Motor by using Modifier. In Proceedings of the 11th International Conference on Optimization of Electrical and Electronic Equipment, 2008 (OPTIM 2008), Brasov, Romania, May 2008; pp. 93-99.

44. Markadeh, G.R.A.; Hajian, M.; Soltani, J.; Hosseinia, S. Maximum Torque Per Ampere Control of Sensorless Induction Motor Drives with DC Offset and Parameter Compensation. *Energy Convers. Manage.* 2010, 51, 1354-1362.
45. Yang, J.; Hu, Y.; Huang, W.; Chu, J.; Gao, J. Direct Torque Control of Brushless DC Motor without Flux Linkage Observation. In Proceedings of the IEEE 6th International Power Electronics and Motion Control Conference, 2009 (IPEMC '09), Wuhan, China, May 2009; pp. 1934-1937.
46. Hajian, M.; Markadeh, G.R.; Soltani, J.; Hoseinnia, S. Energy Optimized Sliding-Mode Control of Sensorless Induction Motor Drives. *Energy Convers. Manage.* 2009, 50, 2296-2306.
47. Zaky, M.S.; Khater, M.; Yasin, H.; Shokralla, S.S. Very Low Speed and Zero Speed Estimations of Sensorless Induction Motor Drives. *Electr. Power Syst. Res.* 2010, 80, 143-151.
48. Dhaouadi, R.; Mohan, N.; Norum, L. Design and Implementation of an Extended Kalman Filter for the State Estimation of a Permanent Magnet Synchronous Motor. *IEEE Trans. Power Electron.* 1991, 6, 491-497.
49. Barut, M. Bi Input-Extended Kalman Filter Based Estimation Technique for Speed-Sensorless Control of Induction Motors. *Energy Convers. Manage.* 2010, 51, 2032-2040.
50. Terzic, B.; Jadric, M. Design and Implementation of the Extended Kalman Filter for the Speed and Rotor Position Estimation of Brushless DC Motor. *IEEE Trans. Ind. Electron.* 2001, 48, 1065-1073.
51. Zaky, M.S.; Khater, M.; Yasin, H.; Shokralla, S.S. Very Low Speed and Zero Speed Estimations of Sensorless Induction Motor Drives. *Electr. Power Syst. Res.* 2010, 80, 143-151.
52. Bose, B.K. Fuzzy Logic and Neural Networks in Power Electronics and Drives. *IEEE Ind. Appl. Mag.* 2000, 6, 57-63.
53. <https://www.electronics-tutorials.ws/blog/optocoupler.html> Available: April 2017
54. W. Brown, "AN857: Brushless DC Motor Control Made Easy", MicroChip Technologies, DS00857A, 2002

APPENDIX

Software for sensored BLDC motor

```
#define hall1 2
#define hall2 3
#define hall3 4

int stepstate;
bool hall1state; // Choose a variable for hall states
bool hall2state;
bool hall3state;

void ExInt0() { // Create an external interrupt
    hall1state = digitalRead(hall1); // Creating the steps for hall sensor
    NextStep();
}

void ExInt1() {
    hall2state = digitalRead(hall2); // Creating the steps for hall sensor
    NextStep();
}

ISR(PCINT2_vect) {
    hall3state = digitalRead(hall3); // Creating the steps for hall sensor
    NextStep();
}

ISR(ADC_vect) {
    int x = ADCH; // read 8 bit value from ADC for potensiometer
    OCR1B = map(x,0,255,1,799);
}

ISR(TIMER1_COMPA_vect) { //Creating Corresponding Commutations steps for BLDC
motor
    switch (stepstate) {
        case 1:
            PORTD = B00100000;
            PORTB = B00000001;
            break;
        case 2:
            PORTB = B00000011;
            break;
        case 3:
            PORTB = B01000000;
            PORTD = B00000010;
            break;
        case 4:
            PORTB = B11000000;
```

```

        break;
    case 5:
        PORTB = B10000000;
        PORTD = B00000100;
        break;
    case 6:
        PORTD = B00100000;
        PORTB = B00000100;
        break;
    }
}

ISR(TIMER1_COMPB_vect) {
    PORTD = B01000000;
    PORTB = B00000101;
}

void NextStep() { //checking the outputs from hall sensors
    if ((hall1state == 1) && (hall2state == 0) && (hall3state == 1)) {
        stepstate = 1;
    }
    if ((hall1state == 0) && (hall2state == 0) && (hall3state == 1)) {
        stepstate = 2;
    }
    if ((hall1state == 0) && (hall2state == 1) && (hall3state == 1)) {
        stepstate = 3;
    }
    if ((hall1state == 0) && (hall2state == 1) && (hall3state == 0)) {
        stepstate = 4;
    }
    if ((hall1state == 1) && (hall2state == 1) && (hall3state == 0)) {
        stepstate = 5;
    }
    if ((hall1state == 1) && (hall2state == 0) && (hall3state == 0)) {
        stepstate = 6;
    }
    TCNT1 = 790;
}

void setup() {
    DDRD = B11100000; //Pin 0,1,2,3,4 Input; Pin 5,6,7 Output
    DDRB = B00000111; //Pin 8,9,10 Output
    TCCR1A = 0;
    TCCR1B = 0;
    TCCR1B |= (1 << WGM12) | (1 << CS10); //CTC Mode, Prescaler 1
    TCNT1 = 0;
    OCR1A = 800;
    OCR1B = 0;
    TIMSK1 = 0;
    TIMSK1 |= (1 << OCIE1B) | (1 << OCIE1A);
}

```

```

ADCSRA = 0;           // clear ADCSRA register
ADCSRB = 0;           // clear ADCSRB register
ADMUX |= (0 & 0x07); // set A0 analog input pin
ADMUX |= (1 << REFS0); // set reference voltage
ADMUX |= (1 << ADLAR); // left align ADC value to 8 bits from ADCH register
ADCSRA |= (1 << ADPS2) | (1 << ADPS1) | (1 << ADPS0); //Prescaler 128
ADCSRA |= (1 << ADATE); // enable auto trigger
ADCSRA |= (1 << ADIE); // enable interrupts when measurement complete
ADCSRA |= (1 << ADEN); // enable ADC
ADCSRA |= (1 << ADSC); // start ADC measurements

PCICR |= 0b00000100; // turn on port d
PCMSK2 |= 0b00010000; // turn on PD4 (D4)
attachInterrupt(0, ExInt0, CHANGE);
attachInterrupt(1, ExInt1, CHANGE);

hall1state = digitalRead(hall1);
hall2state = digitalRead(hall2);
hall3state = digitalRead(hall3);
}

void loop() {
}

```

The code is firstly waiting for the state change of the one of hall sensors. If one happens, the Arduino determines which step needs to be activated then timer one activates the corresponding MOSFETs of the step. After certain amount of time which is determined by the potentiometer. Timer 1 connects all phases one to another and take a quick brake before to power the phases ones again. This creates PWM signal, which lowers the average voltage and lowers the current, lowering the magnetic force and rotation speed. This process continues until there is another Hall Effect sensor state change, which activates the next step.